Project report

FF2021-1040 Cost Effective Methods of Installing Offshore Wind Infrastructure

Authors:
Dr. Rodrigo Martinez
Dr. Marcin Kapitaniak
Professor Richard Neilson
Dr. Sergi Arnau

31st July 2022

Contents

Executive summary

The purpose of this report is to provide a report of the project FF2021-1040 Cost Effective Methods of Installing Offshore Wind Infrastructure. Summary of the milestones achieved and activities undertaken in the period from 1st June 2021 to 30th of July 2022 is listed below:

- Simulations
    - Buoyancy characterisation simulations of the anchor using a range of ballast pumping rates.
    - Positioning the anchor under the stern of the vessel using a range of ballast pumping rates.
    - Controlled descent of the vessel under a range of wave heights and flow velocities.
    - Comparison between suction anchors and variable buoyancy anchors
- Dissemination
    - Participation at NDC and school seminars.
    - Participation at international conferences (WMVC and PRIMaRE).
    - Preparation of journal paper (Ocean Engineering).

1 Introduction

The economic drivers for lowering CapEx and OpEx of floating offshore wind technologies calls for innovation. In this study, the feasibility of deploying a novel type of anchor with variable buoyancy for mooring floating offshore wind turbines is presented. A set of detailed modelling studies are performed it the state-of-the-art, Marine Simulator at the National Decommissioning Centre (NDC). Using the multi-physics simulator allows for a more economical proof-of-concept approach. This will allow to fully assess the proposed deployment method and de-risk future offshore deployments. By using the proposed floating anchor, the use of heavy-lifting cranes and vessels is intended to be avoided, thereby reducing complexity and associated expenses. Instead, the anchor can be deployed from a smaller vessel, equipped with a simple winch. Once the anchor is towed to the deployment site, the anchor is pumped with liquid ballast and lowered with the winch. The proposed anchor (Figure 1) has the shape of a truncated pyramid with a 10 m square base and is 4.46 m high (eye-bolt inclusive). The empty anchor has a weight of 163 tonnes.

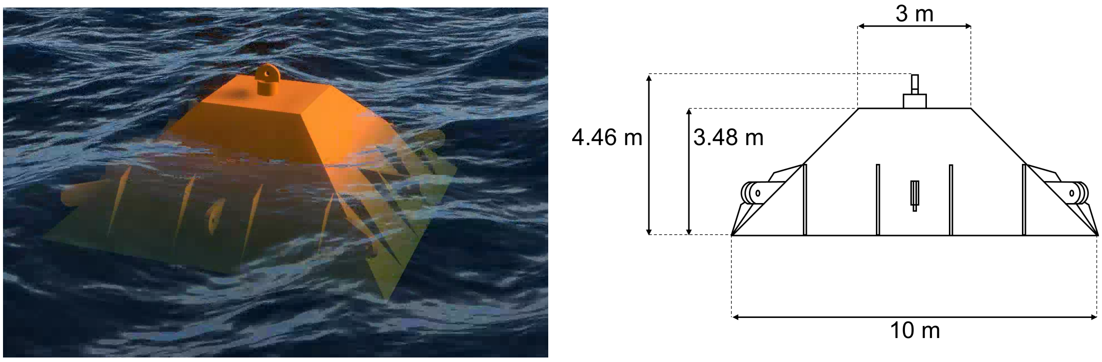

Figure 1: Left: 3D representation of the anchor in the simulator's environment. Right: 2D diagram of the anchor.

2 State of the art

This section provides an insight to the current state of the deployment of offshore wind turbines, their moorings and anchors as well as the typical weather conditions in which offshore deployments are performed.

2.1 Floating offshore wind turbines

Offshore wind turbines can be divided in two categories: floating and fixed to the seabed. Much of the offshore wind energy resource worldwide is located over deep water and current fixed-bottom turbine technology may not be an economical solution for harvesting this deep water resource. Floating offshore wind turbines allow this resource to be harnessed [1]. Floating turbines are classified in four predominant types: semi-submersible, tension-leg-platform (TLP), spar and, barge platforms. All of these require anchors to be moored to the seabed. Regardless of the anchor type, deployments are usually proposed using established anchoring technologies/methodologies borrowed from the O&G industry [2]. At the time of writing, no literature was found on the development of novel anchoring technologies despite its potential for improvement [3, 4, 5].

2.2 Anchor deployment

Little information is found related to the type of anchor employed for floating wind. However, knowledge from the Oil & Gas industry is adapted to meet the offshore wind requirements [6, 7]. Figure 2 shows the most common anchors used for floating wind turbines [6]. In comparison with other types of anchors, gravity anchors (d) require medium to hard soils, their main loading direction is vertical but can perform at different angles. A drawback of gravity anchors is the weight for which they rely to work efficiently. This heavy weight increases installation costs and decreases the potential to recover the anchors upon decommissioning. Each type of anchor has its own deployment procedure. Drag-embedded (a) and gravity anchors (d) are simply lowered to the seabed. Whereas driven (b) and suction (c) piles need further interventions for their installation. The selection criteria for anchors is highly dependant on the seabed conditions of the deployment location. Hence, bathymetry surveys should be conducted as part of the planning process.

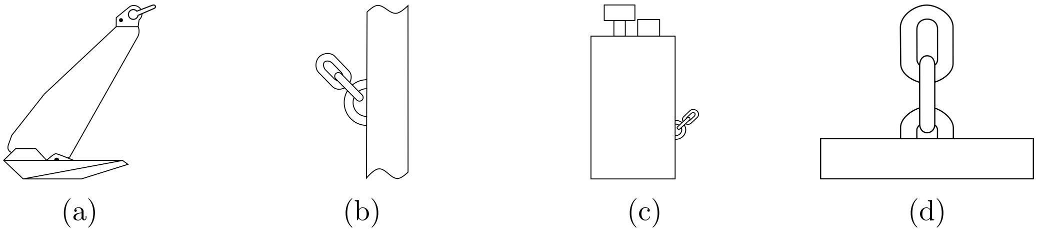
(a) (b) (c) (d)

Figure 2: Anchor types generally used in floating offshore turbines: a) drag-embedded, b) driven pile, c) suction pile, d) gravity anchor. Adapted from [6].

2.3 Flow characteristics and weather window

Offshore deployment is limited by so-called weather windows. These weather windows are characterised by a series of environmental conditions that allow for the safe deployment of equipment [8, 9]. The main characteristics associated to weather windows are the significant wave height (H_S) and flow velocity (U). Average flow velocity around the North Sea is usually below 1m/s ($\sim$ 2 kn) [10, 11]; however, in certain areas characterised by channels, straits or some other land features, can reach up to 4 m/s ($\sim$ 8 kn)[12, 13].

3 Methodology

The 3D CAD model of the proposed anchor is imported into the OSC simulator software with its corresponding collision model. The schematic of the anchor is depicted on Figure 3 (left). The anchor has a square base with 10.00 m sides and height of 3.48 m (4.46 m including eye bolt). The anchor has a weight of 163.20 t. The inertia properties of the steel anchor are calculated based on the CAD drawing. They are then imported into the OSC simulator as part of the collision model generation process. Collision model generation is based on creating a mesh structure to represent the anchor. It is generated using the software 3DS Max before importing it into the OSC simulator. Due to the simulator only taking into account the volume of the steel plates and internal bulkheads used to create the anchor shape, it is necessary to create a solid part that will represent the inner volume of the anchor (Figure 3 (right)). This inner volume is filled/emptied to modify the anchor's buoyancy. The inner volume is fixed to the anchor within the simulator environment. The model of the anchor is assembled in the OSC simulator with the two components depicted in Figure 3, where the inner volume representing the air/liquid is fixed rigidly inside the anchor. In order to ensure that the anchor floats, the inner volume is assigned a mass of 170 kg, which corresponds to the weight of the inner volume of 142.44 m^3 filled with air. The anchor is connected to the hose reel, using a standard 4" hose and a 50 mm outside diameter (OD) steel winch cable.

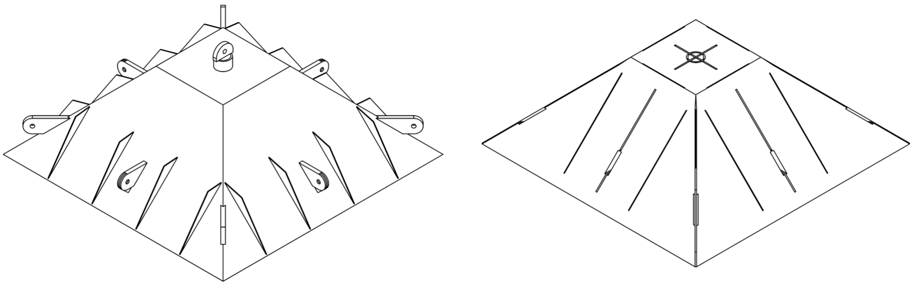

Figure 3: 3D model of the anchor (left) and the internal representation (right).

The anchor deployment process is shown in Figure 4. The developed scenario assumes that the floating anchor will be towed to the site and deployed from a support vessel equipped with a winch and a hose reel. As shown in Figure 4.1, the floating anchor is connected to the winch using a cable and through a hose to the reel. Through the hose, the ballast fluid is pumped into the anchor. Once the anchor has negative buoyancy, the anchor starts sinking and positions itself under the stern of the vessel, eventually hanging from the winch cable (Figure 4.2). At this point, the anchor starts its controlled descent to the seabed guided by the winch at the desired velocity (Figure 4.3).

In the simulation scenario the anchor is deployed in 100 m water depth. Ocean conditions are represented by irregular waves with a JONSWAP spectrum. Significant wave heights (H_S) explored ranged from 1 to 5 m with peak period (T_P) of 10 s and, currents ranging from 0.1 to 1.0 kn.

3.1 JOWNSAP irregular wave spectrum

The JOWNSAP Spectrum S_j gives and approximation of the distribution of wave energy among different wave frequencies of wave-lengths on the sea surface. It was proposed by Hasselmann et al. [14] and it is a modified spectra version of the Pierson-Moskowitz Spectrum S_p [15], in which a peak enhancement factor is added

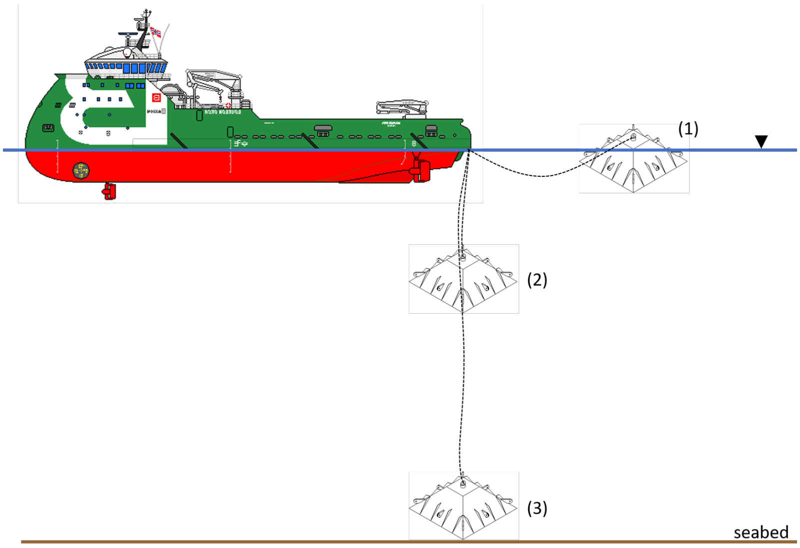

Figure 4: Schematic of the deployment process of the anchor: (1) initial position of the anchor after towing. Pumping of ballast commences to generate negative buoyancy. (2) positioning of the anchor underneath the vessel's stern. (3) controlled descent of the anchor by means of a simple winch.

(γ^r) as the wave spectrum is never fully developed through wave-wave interactions (Figure 5).

$$S_j\left(\omega\right)=\frac{\alpha g^2}{\omega^5}\exp\left[-\frac{5}{4}\left(\frac{\omega_p}{\omega}\right)^4\right]\gamma^r \tag{1}$$

where g is the acceleration due to gravity, $\omega = 2\pi f$ (where f is the wave frequency [Hz]), $\sigma = 8.1\times10^{-3}$,

$$r=\exp\left[-\frac{\left(\omega-\omega_p\right)^2}{2\sigma^2\omega_p^2}\right] \tag{2}$$

and

$$\sigma=\begin{cases}\sigma_1=0.07, & \text{for } \omega\leq\omega_p.\\ \sigma_2=0.09, & \text{for } \omega>\omega_p.\end{cases} \tag{3}$$

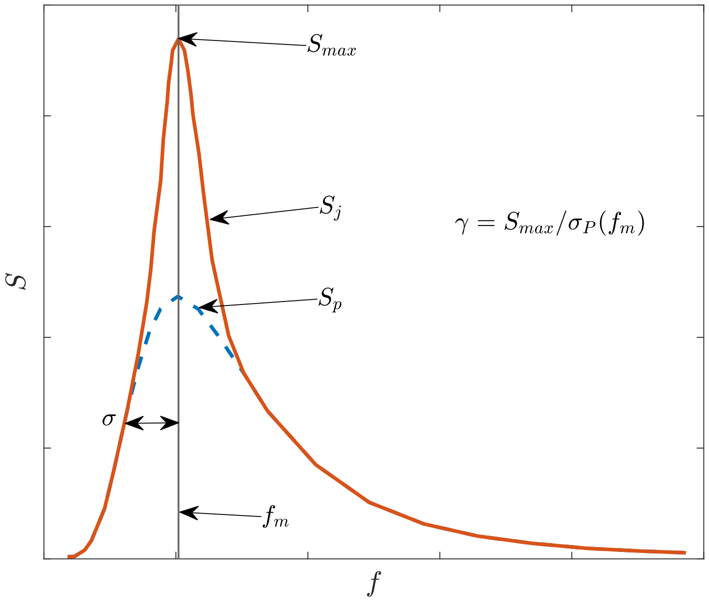

Figure 5: Comparison between JONSWAP Spectrum S_j and Pierson-Moskowitz Spectrum S_p. The difference between maximum values is due to the added peak enhancement factor.

4 Results

The analysis of the deployment process is divided in three sections: 1.- characterisation of the anchor's buoyancy, 2.- positioning the anchor under the stern of the vessel by pumping ballast into the anchor to create negative buoyancy and, 3.- the controlled/guided descent of the anchor to the seabed by a winch.

4.1 Buoyancy

To determine the buoyancy limit of the anchor when filled with air, the mass of the anchor is increased until the anchor is fully submerged. This is achieved by increasing the rate at which the ballast is pumped into the anchor (Q). Table 1 enlists all the Q values used in the buoyancy tests.

The anchor buoyancy characterisation is shown in Figure 6, where each curve corresponds to a specific pump rate. The vertical dashed line corresponds to the actual mass of the anchor (163.2 t), while the two horizontal dashed lines denote the anchor body height (3.48 m) and overall anchor height (4.46 m), respectively. As shown, the buoyancy characteristics of the anchor change when the draft reaches the lower dashed line (167.3 t), which means that the anchor body is fully submerged and only the lifting hook remains above the water level. After this point there is a sharp change in the buoyancy characteristics and the precise buoyancy limit can be determined from the crossing point between the curve and the top horizontal line (lifting hook at the water level). When the anchor mass reaches between 167 and 168 t, depending on the pump rate, the anchor becomes neutrally buoyant. This

Table 1: Buoyancy parameters

Case	Q [m^3/min]	Case	Q [m^3/min]
1	0.04	11	1.07
2	0.09	12	1.07
3	0.17	13	1.24
4	0.26	14	1.33
5	0.34	15	1.37
6	0.47	16	1.37
7	0.60	17	1.45
8	0.73	18	1.62
9	0.85	19	1.87
10	1.02		

means that anchor possesses a gross buoyancy of about 4 t. The difference between the different pump rates is attributed to the inertia created by the speed at which the ballast is being pumped.

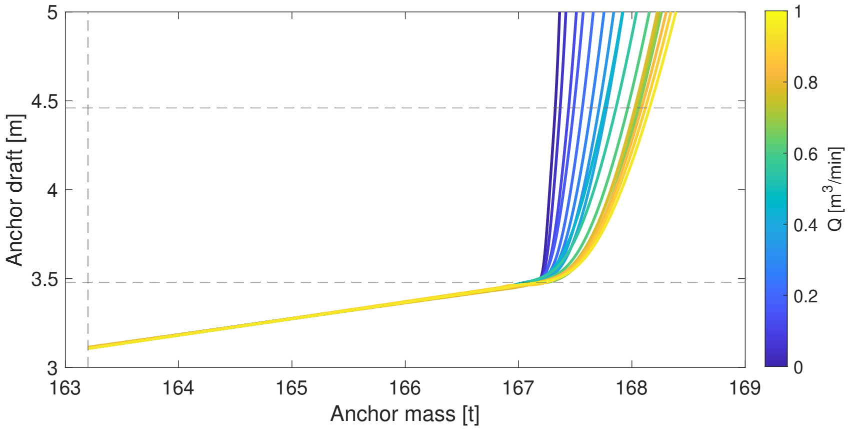

Figure 6: Anchor buoyancy tests as a function of pump flow rate Q. Vertical line represents the weight of the anchor in air. The bottom horizontal line represent the height of the anchor without eye-bolt, the top line takes into consideration the height of the eye-bolt.

4.2 Positioning

The tests positioning the vessel underneath the vessel stern are analysed as a function of the pump rate Q (m^3/min). A range of H_S values is also explored. Tables 2 and 3 show the parameter combinations for all the positioning tests performed.

The variation of the winch force (F_W), anchor vertical position (Z_A) with the pump rate (Q) are shown in Figure 7 (left). Vertical dashed lines indicate the time at which F_W and Z_A stabilise. At faster pump rates (Q≈1 m^3/min), the anchor can be positioned underneath the stern of the vessel in under 5 minutes. In contrast, at slower pump rates (Q≈0.05 m^3/min), the anchor takes up to 35 minutes to position under the vessel. Due to the length of the cable, the forces acting on the winch cable

(F_W) remain constant until the anchor is roughly 18 m under the water surface. The anchor 3D trajectory from the surface to underneath the vessel is shown in Figure 7 (right). At the lowest pump rate, the trajectory presents oscillations compared to the other pump rates. This is thought to be associated to the time it takes for the anchor to reach the bottom of the vessel, making it more susceptible to wave-induced effect.

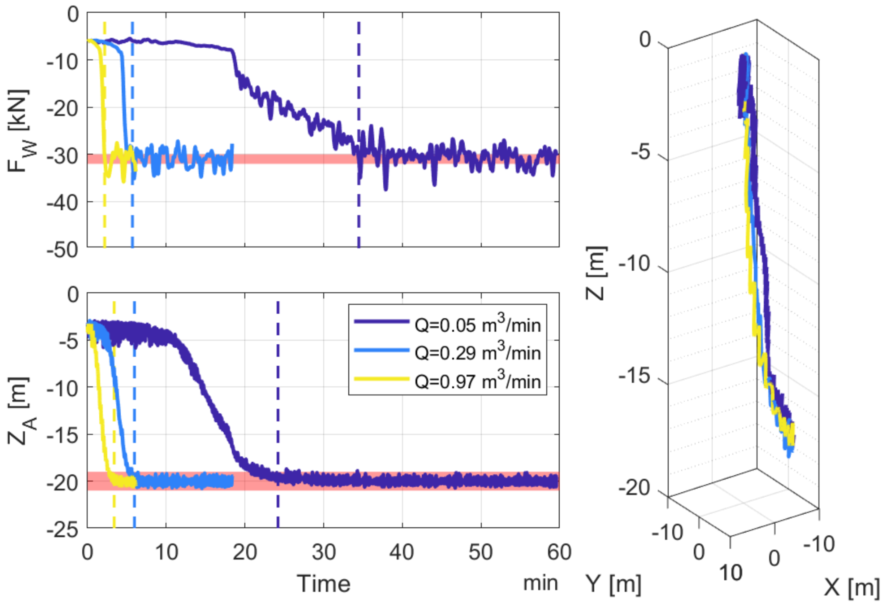

Figure 7: Winch force (top) and anchor vertical position (bottom) for Q=0.05, 0.29 and 0.97 m^3/min. Vertical dashed lines represent the time at which the signals stabilise.

Comparing the settling times of the winch force and anchor sinking velocity is shown in Figure 8 for all pump rates Q. At Q=0.5 m^3/min, the anchor reaches its position under the stern around 10.5 minutes before the winch force stabilises. This means that once the anchor is in position, the ballast gets pumped for a further 10 minutes. In contrast, at higher Q, the pump stops a couple of minutes before the anchor has reached its position. At Q=0.4 m^3/min, both F_W and Z_A settle in 4.8 minutes. From this point, as pump rate increases, settling times decrease at a lower rate. At Q=1 m^3/min F_W settles in 1.9 minutes and Z_A settles in 2.9 minutes.

The force excerpted on the winch during the positioning of the anchor under the stern of the vessel is recorded in Figure 9. At the pump rates Q tested, there does not seem to be mayor changes in the force with the average being 60 kN. There are some force values at Q=0.08, 0.8 and 1.05 m^3/min that reach 100 kN but no indication whether they are outliers or real data has been identified.

Wave-induced oscillations are shown in Figure 10. It is clear that the anchor's vertical position Z_A is influenced by the wave motion. For $H_S = 1$ m, the anchor does not oscillate as much during its descent between 10 and 15 m. On the other hand, waves with $H_S = 3$ m induce oscillations in the anchor's vertical position at all times, having the largest oscillations amplitude of the three examples.

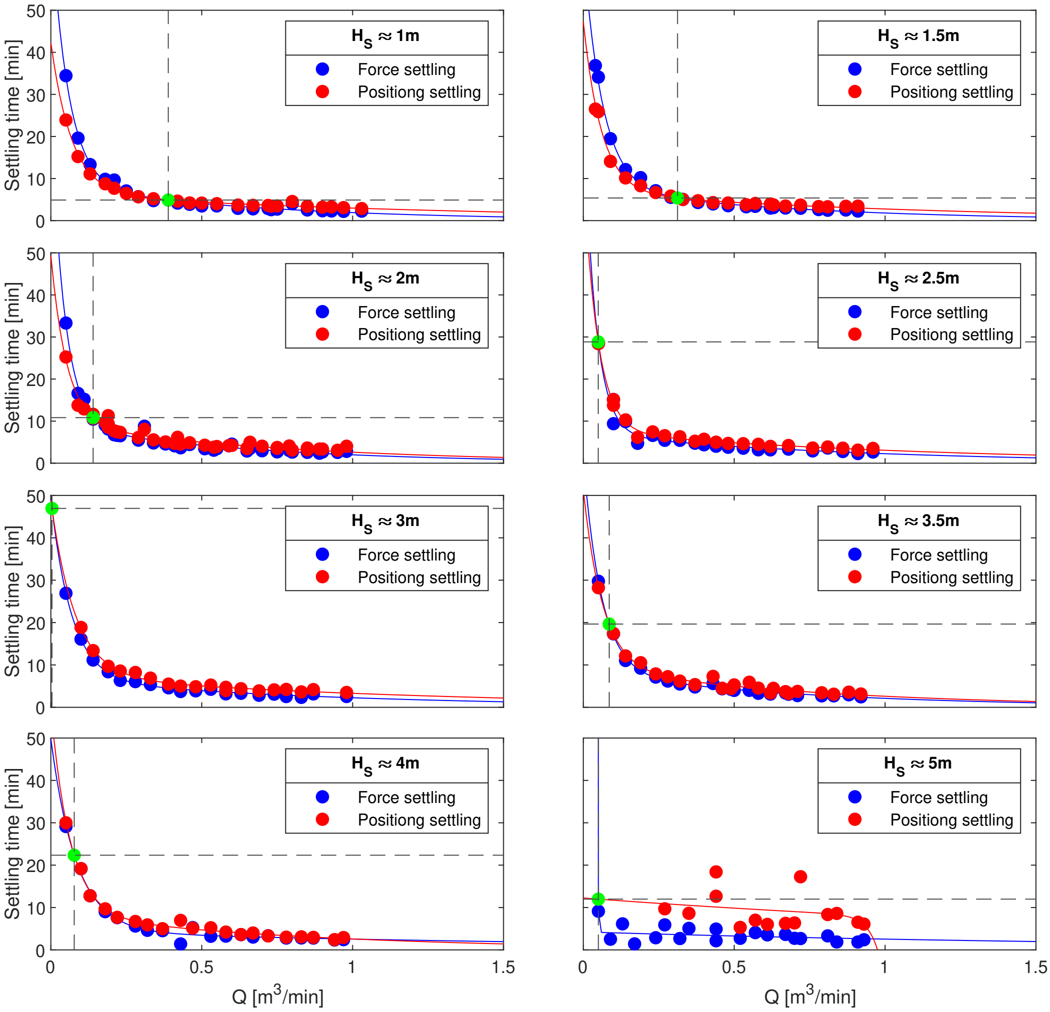

Figure 8: Variation of anchor positioning settling time with pump rate Q. Exponential curves fitted.

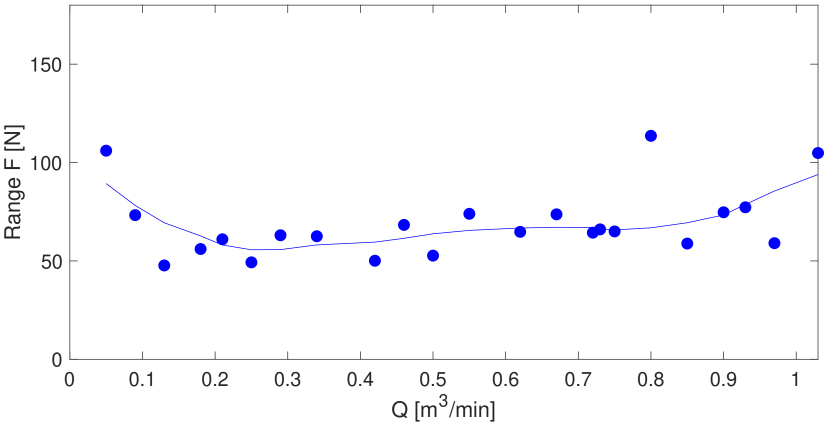

Figure 9: Variation of winch force with pump rate Q. Exponential curves fitted.

Table 2: Positioning parameters

Case	**Q [m^3/min]**	**H$_S$ [m]**	**T [s]**
1	0.05	1.0	10
2	0.09	1.0	10
3	0.13	1.0	10
4	0.18	1.0	10
5	0.21	1.0	10
6	0.25	1.0	10
7	0.29	1.0	10
8	0.34	1.0	10
9	0.42	1.0	10
10	0.46	1.0	10
11	0.50	1.0	10
12	0.55	1.0	10
13	0.62	1.0	10
14	0.67	1.0	10
15	0.72	1.0	10
16	0.73	1.0	10
17	0.75	1.0	10
18	0.80	1.0	10
19	0.85	1.0	10
20	0.90	1.0	10
21	0.93	1.0	10
22	0.97	1.0	10
23	1.03	1.0	10
24	0.04	1.5	10
25	0.05	1.5	10
26	0.09	1.5	10
27	0.14	1.5	10
28	0.19	1.5	10
29	0.19	1.5	10
30	0.24	1.5	10
31	0.29	1.5	10
32	0.33	1.5	10
33	0.38	1.5	10
34	0.43	1.5	10
35	0.48	1.5	10
36	0.54	1.5	10
37	0.57	1.5	10
38	0.62	1.5	10
39	0.63	1.5	10
40	0.67	1.5	10
41	0.72	1.5	10
42	0.78	1.5	10
43	0.81	1.5	10
44	0.87	1.5	10
45	0.91	1.5	10
46	0.05	2.0	10
47	0.09	2.0	10
48	0.14	2.0	10
49	0.19	2.0	10
50	0.23	2.0	10
51	0.29	2.0	10
52	0.34	2.0	10
53	0.38	2.0	10
54	0.41	2.0	10
55	0.46	2.0	10
56	0.51	2.0	10
57	0.55	2.0	10
58	0.60	2.0	10
59	0.65	2.0	10
60	0.70	2.0	10
61	0.75	2.0	10
62	0.75	2.0	10
63	0.80	2.0	10
64	0.85	2.0	10
65	0.90	2.0	10
66	0.95	2.0	10
67	0.05	2.5	10
68	0.05	2.5	10
69	0.10	2.5	10
70	0.10	2.5	10
71	0.14	2.5	10
72	0.18	2.5	10
73	0.23	2.5	10
74	0.27	2.5	10
75	0.29	2.5	10
76	0.32	2.5	10
77	0.37	2.5	10
78	0.40	2.5	10
79	0.44	2.5	10
80	0.48	2.5	10
81	0.53	2.5	10
82	0.58	2.5	10
83	0.62	2.5	10
84	0.68	2.5	10
85	0.76	2.5	10
86	0.81	2.5	10
87	0.86	2.5	10
88	0.91	2.5	10
89	0.96	2.5	10

Table 3: Positioning parameters

Case	**Q [m^3/min]**	**H$_S$ [m]**	**T [s]**
90	0.05	3.0	10
91	0.10	3.0	10
92	0.14	3.0	10
93	0.19	3.0	10
94	0.23	3.0	10
95	0.28	3.0	10
96	0.33	3.0	10
97	0.39	3.0	10
98	0.43	3.0	10
99	0.48	3.0	10
100	0.53	3.0	10
101	0.58	3.0	10
102	0.58	3.0	10
103	0.63	3.0	10
104	0.69	3.0	10
105	0.74	3.0	10
106	0.78	3.0	10
107	0.83	3.0	10
108	0.87	3.0	10
109	0.98	3.0	10
110	0.00	3.5	10
111	0.05	3.5	10
112	0.10	3.5	10
113	0.10	3.5	10
114	0.14	3.5	10
115	0.19	3.5	10
116	0.24	3.5	10
117	0.28	3.5	10
118	0.32	3.5	10
119	0.37	3.5	10
120	0.43	3.5	10
121	0.46	3.5	10
122	0.49	3.5	10
123	0.50	3.5	10
124	0.55	3.5	10
125	0.58	3.5	10
126	0.62	3.5	10
127	0.63	3.5	10
128	0.67	3.5	10
129	0.68	3.5	10
130	0.71	3.5	10
131	0.79	3.5	10
132	0.83	3.5	10
133	0.88	3.5	10
134	0.92	3.5	10
135	0.05	4.0	10
136	0.10	4.0	10
137	0.13	4.0	10
138	0.18	4.0	10
139	0.22	4.0	10
140	0.28	4.0	10
141	0.32	4.0	10
142	0.37	4.0	10
143	0.43	4.0	10
144	0.47	4.0	10
145	0.53	4.0	10
146	0.58	4.0	10
147	0.63	4.0	10
148	0.67	4.0	10
149	0.72	4.0	10
150	0.78	4.0	10
151	0.83	4.0	10
152	0.87	4.0	10
153	0.94	4.0	10
154	0.97	4.0	10
155	0.05	5.0	10
156	0.09	5.0	10
157	0.13	5.0	10
158	0.17	5.0	10
159	0.24	5.0	10
160	0.27	5.0	10
161	0.32	5.0	10
162	0.35	5.0	10
163	0.44	5.0	10
164	0.44	5.0	10
165	0.52	5.0	10
166	0.57	5.0	10
167	0.61	5.0	10
168	0.67	5.0	10
169	0.70	5.0	10
170	0.72	5.0	10
171	0.81	5.0	10
172	0.84	5.0	10
173	0.91	5.0	10
174	0.93	5.0	10

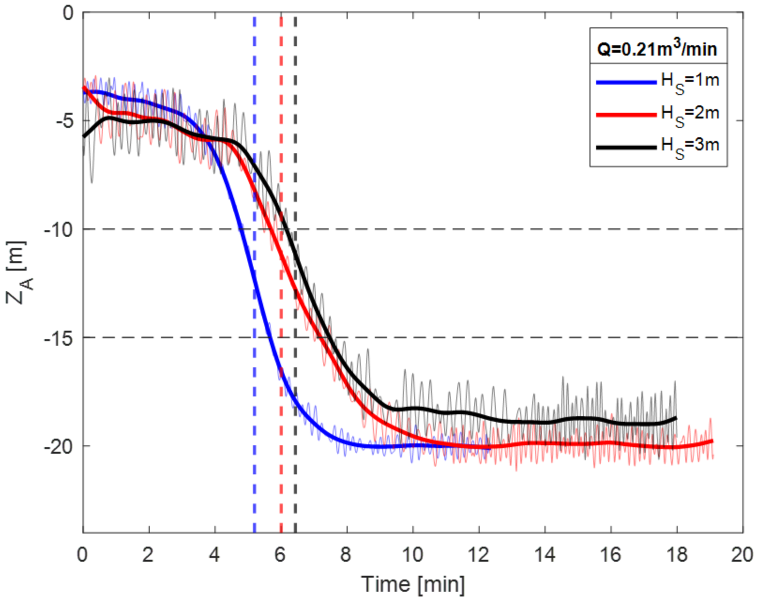

Figure 10: Anchor vertical position as a function of time. For H_S=1, 2 and 3 m.

4.3 Descent - Base case

In contrast to the positioning tests, the anchor descent tests are analysed as a function of the winch velocity V_W (m/s). Table 4 shows all the test matrix used for the descent tests.

Table 4: Descent parameters

Case	V_W [m/s]	H_S [m]	T [s]
1	0.025	1	10
2	0.040	1	10
3	0.050	1	10
4	0.060	1	10
5	0.075	1	10
6	0.090	1	10
7	0.100	1	10
8	0.125	1	10
9	0.150	1	10
10	0.160	1	10
11	0.170	1	10
12	0.175	1	10
13	0.180	1	10
14	0.190	1	10
15	0.200	1	10
16	0.210	1	10
17	0.220	1	10
18	0.225	1	10
19	0.250	1	10
20	0.260	1	10

Case	V_A [m/s]	H_S [m]	T [s]
21	0.270	1	10
22	0.275	1	10
23	0.290	1	10
24	0.300	1	10
25	0.300	1	10
26	0.310	1	10
27	0.320	1	10
28	0.325	1	10
29	0.330	1	10
30	0.340	1	10
31	0.350	1	10
32	0.350	1	10
33	0.360	1	10
34	0.375	1	10
35	0.380	1	10
36	0.400	1	10
37	0.425	1	10
38	0.450	1	10
39	0.475	1	10
40	0.500	1	10

Initial tests did not include heave compensation. The anchor vertical position Z_A and winch force F_W are directly impacted by the wave motion. This influence increases the average winch force by up to 3 times and also increases the descent time as the anchor starts and stops with its heaving motion.

From these initial tests, a simple heave compensation system consisting of an axial spring of stiffness $k_z = 1000\,\frac{\mathrm{kN}}{\mathrm{m}}$ was added to the simulation (Figure 11), which reduced the spikes experienced in the winch force.

Figure 12 shows the effect of waves on the anchor's vertical position and winch force using heave compensation. Results are for three winch velocity values. It can be seen that there are no spikes in the force signal associated to the pulling of the cable. Wave-induced oscillations in Z_A reduce in amplitude and period as the winch velocity increases. Similar behaviour is seen in the F_W data, average force also reduces with the increase in V_W.

A range of winch velocities, associated forces acting on the winch cable, along with the three-dimensional anchor descent trajectories and orientation are carefully analysed. Similar behaviour can be seen in Figure 13, where the deployment time stabilises above 0.35 m/s.

Time histories of the anchor's vertical position are presented in figure 14. In this Figure, it can be seen that the slowest it takes for the anchor to reach the seabed

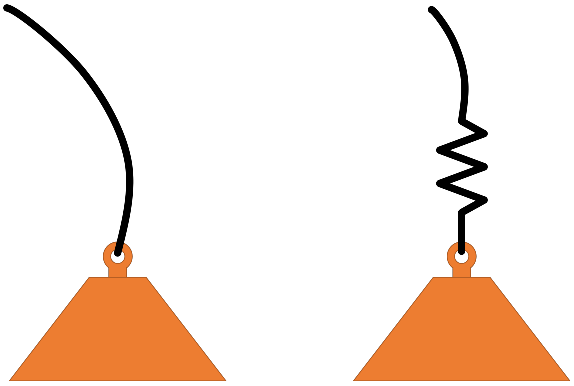

Figure 11: Left: simple model of anchor and cable. Right: representation of the heave compensation mechanisms using an axial spring of stiffness $k_z = 1000\,\frac{\mathrm{kN}}{\mathrm{m}}$ in the simulator.

is 4 minutes. This time is for the slowest winch velocity of 0.3 m/s. For the fastest winch velocities, the anchor reaches the seabed just above 3.5 minutes.

The X and Y position are now analysed in figure 15. With the lack of current, it is natural that at all winch speeds the landing position of the anchor would be very similar at all winch speeds. This is seen in the X position, where the anchor stays ±1 m from the initial position. for the case of the Y direction, there is a larger drift but this is associated to the wave direction. In this case, the anchor drifts up to 10 m from the landing position.

The sinking trajectories are shown in Figure 16. The trajectory is similar at all winch velocities. However, the slower the descent, the further the anchor drifts from its initial position (up to 10 m in the Y direction).

In Figure 17, the anchor descent velocity is plotted against the winch velocities considered. It can be seen that for V_W values below 0.35 m/s the anchor descent is governed by the winch. However, at higher V_W values, the anchor reaches an equilibrium and it's descent velocity does not increase (free fall), regardless of the winch velocity.

The orientation range of the anchor is shown in Figure 24 (right). The yaw range is the difference between the yaw angle at the time the anchor reaches the seabed and the angle the winch is released. For pitch and roll, which are only influenced by the waves, the range is the difference between the maximum and minimum values in the time series. During the anchor's descent, roll is kept almost constant at all winch velocities, with a standard deviation of 0.6°. Pitch has more variation as winch velocity increases, with a standard deviation of 1.7°. However, in the considered range of winch velocities, the anchor's rotation about its vertical axis (yaw) presents a standard deviation of 10°.

Winch force (F_W) results from Figure 19 indicate that, in the presence of passive heave compensation, the working load amplitude on the winch cable decreases from 80 kN at the lowest winch velocities to about 30 kN for winch velocities above 0.35 m/s. The spread visible in the force data is associated to the wave-induced heave oscillations of the anchor and the vessel.

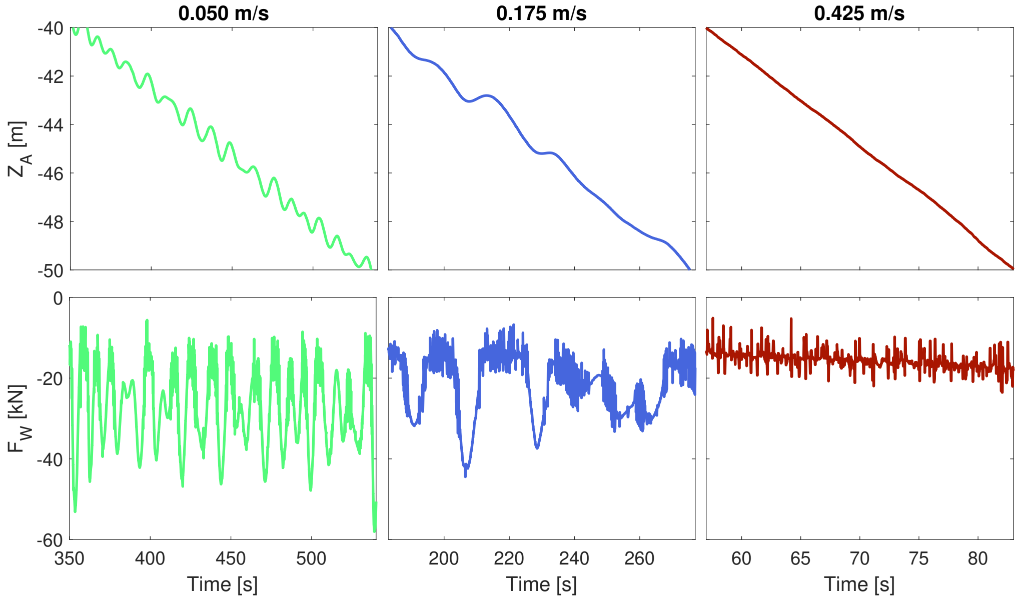

Figure 12: Effect of waves on the anchor and winch forces. Top: Anchor vertical position Z_A. Bottom: Winch force F_W. For three different winch velocities V_W.

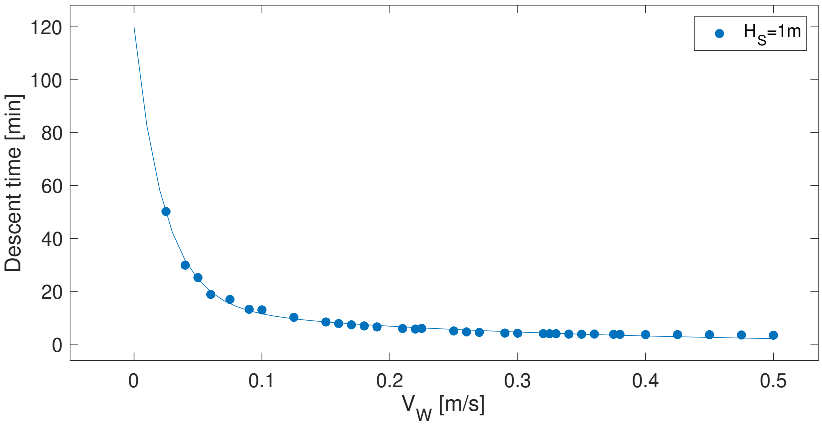

Figure 13: Descent time as a function of winch velocity.

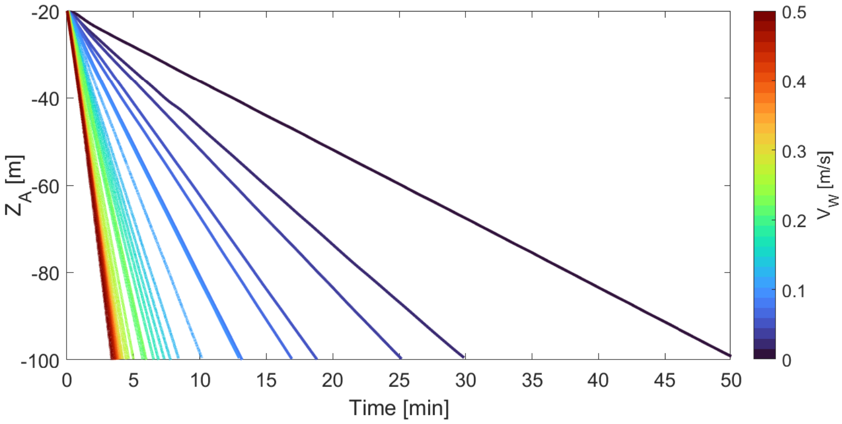

Figure 14: Variation of the anchor's vertical position with time for H_S =1 m.

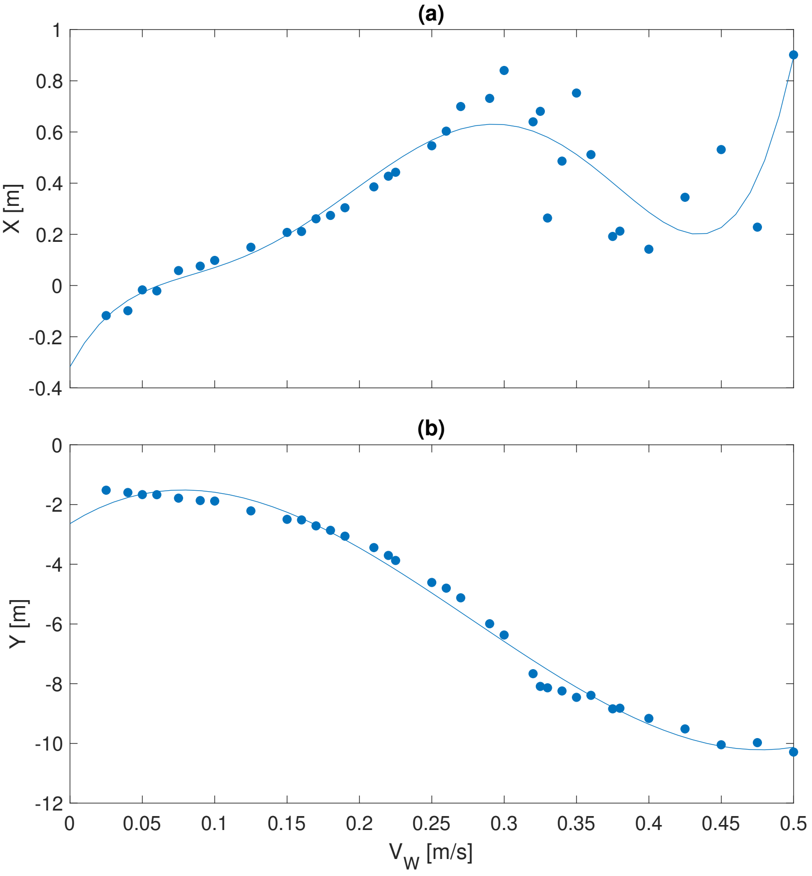

Figure 15: Winch force range (top-left) and descent time (bottom-left) as a function of winch velocity and 3D descent trajectory (centre). Ranges of angular displacements of the anchor in yaw, pitch and roll directions (right).

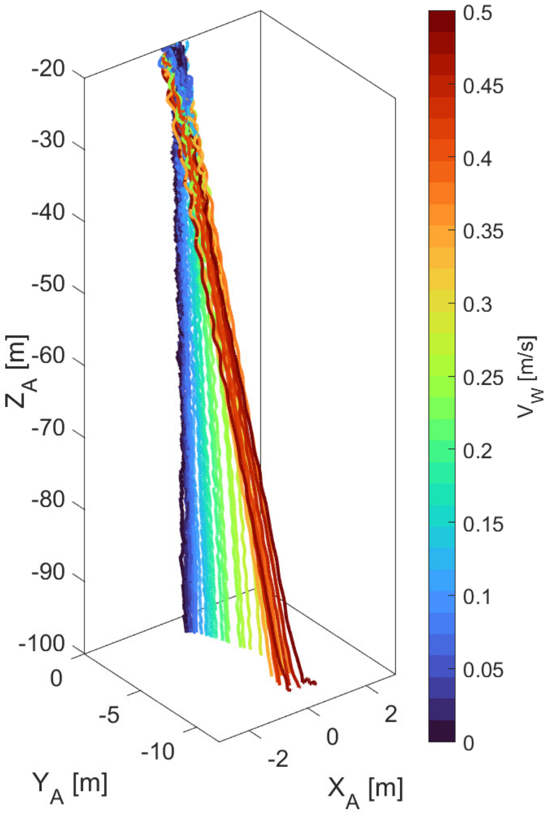

Figure 16: 3D descent trajectory of the anchor for wave case H_S =1 m.

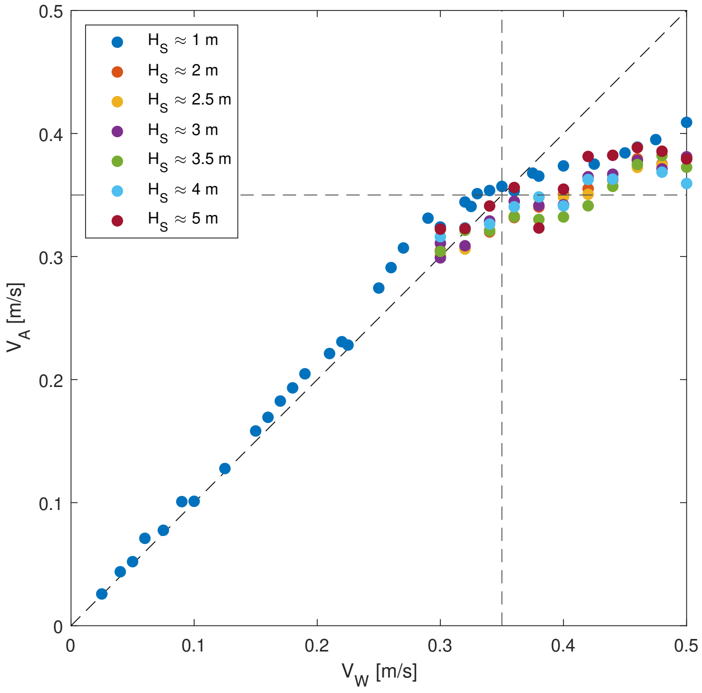

Figure 17: Variation of the anchor deployment speed (V_A) with the winch speed (V_W).

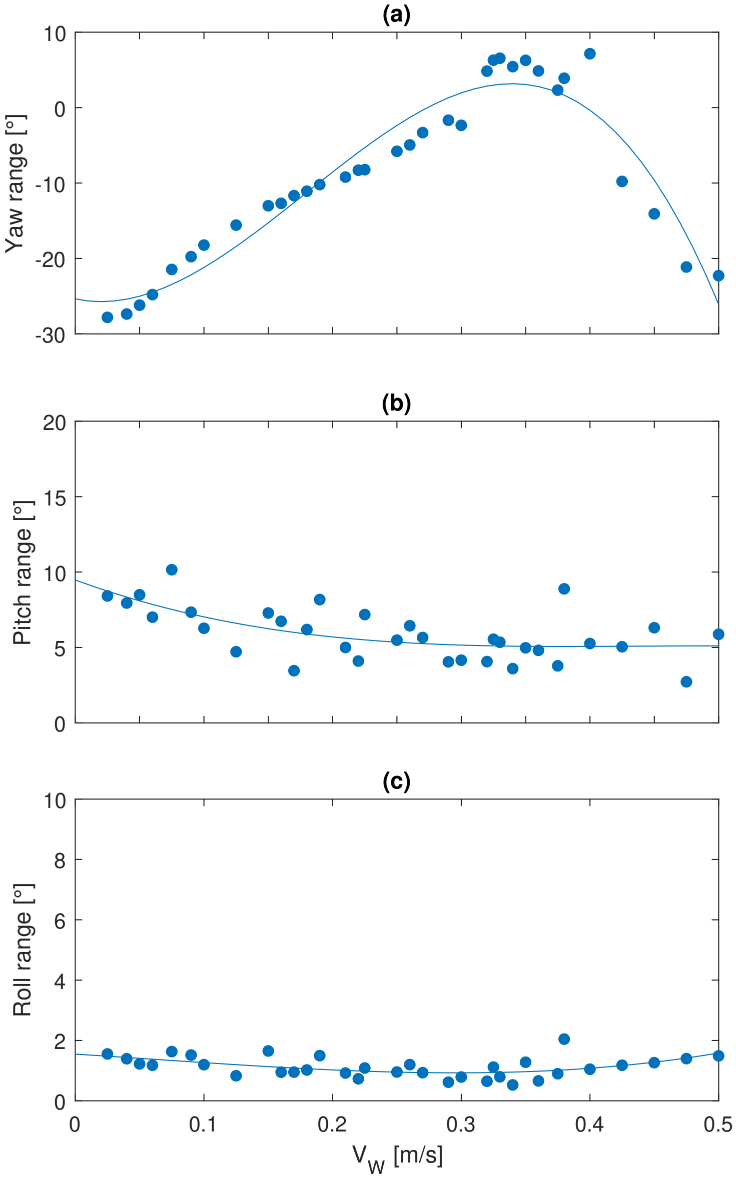

Figure 18: Winch force range (top-left) and descent time (bottom-left) as a function of winch velocity and 3D descent trajectory (centre). Ranges of angular displacements of the anchor in yaw, pitch and roll directions (right).

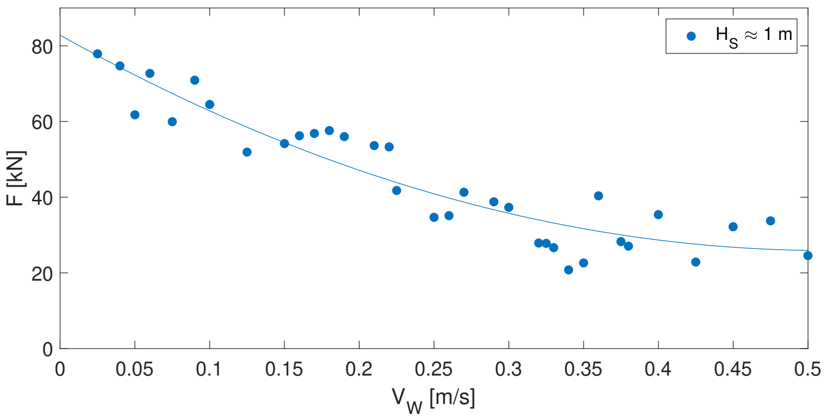

Figure 19: Winch force range as a function of winch velocity.

4.4 Descent - Effects of wave height

After exploring the original range of winch velocities, and an ideal winch speed is observed (V_W =0.35 m/s), the effect of a range of significant wave heights is analysed around this winch velocity. The extent of tests performed is shown in Table 5.

Table 5: Descent parameters

Case	**V_A [m/s]**	**H_S [m]**	**T [s]**
1	0.30	2.0	10
2	0.32	2.0	10
3	0.34	2.0	10
4	0.36	2.0	10
5	0.38	2.0	10
6	0.40	2.0	10
7	0.42	2.0	10
8	0.44	2.0	10
9	0.46	2.0	10
10	0.48	2.0	10
11	0.50	2.0	10
12	0.30	2.5	10
13	0.32	2.5	10
14	0.34	2.5	10
15	0.36	2.5	10
16	0.38	2.5	10
17	0.40	2.5	10
18	0.42	2.5	10
19	0.44	2.5	10
20	0.46	2.5	10
21	0.48	2.5	10
22	0.50	2.5	10
23	0.30	3.0	10
24	0.32	3.0	10
25	0.34	3.0	10
26	0.36	3.0	10
27	0.38	3.0	10
28	0.40	3.0	10
29	0.42	3.0	10
30	0.44	3.0	10
31	0.46	3.0	10
32	0.48	3.0	10
33	0.50	3.0	10
34	0.30	3.5	10
35	0.32	3.5	10
36	0.34	3.5	10
37	0.36	3.5	10
38	0.38	3.5	10
39	0.40	3.5	10
40	0.42	3.5	10
41	0.44	3.5	10
42	0.46	3.5	10
43	0.48	3.5	10
44	0.50	3.5	10
45	0.30	4.0	10
46	0.32	4.0	10
47	0.34	4.0	10
48	0.36	4.0	10
49	0.38	4.0	10
50	0.40	4.0	10
51	0.42	4.0	10
52	0.44	4.0	10
53	0.46	4.0	10
54	0.48	4.0	10
55	0.50	4.0	10
56	0.30	5.0	10
57	0.32	5.0	10
58	0.34	5.0	10
59	0.36	5.0	10
60	0.38	5.0	10
61	0.40	5.0	10
62	0.42	5.0	10
63	0.44	5.0	10
64	0.46	5.0	10
65	0.48	5.0	10
66	0.50	5.0	10

Descent times for all wave heights is shown in figure 20. The longest it takes for the anchor to reach the seabed is under 5 minutes for the highest waves. On average, cases with $H_S = 5$ m, take roughly 0.3 minutes (or 18 seconds) longer that the cases with $H_S = 1$ m (Figure 13).

Similar to Figure 14, Figure 21 shows the vertical position of the anchor but for all wave heights. Each panel represents the data obtained at all winch velocities for a

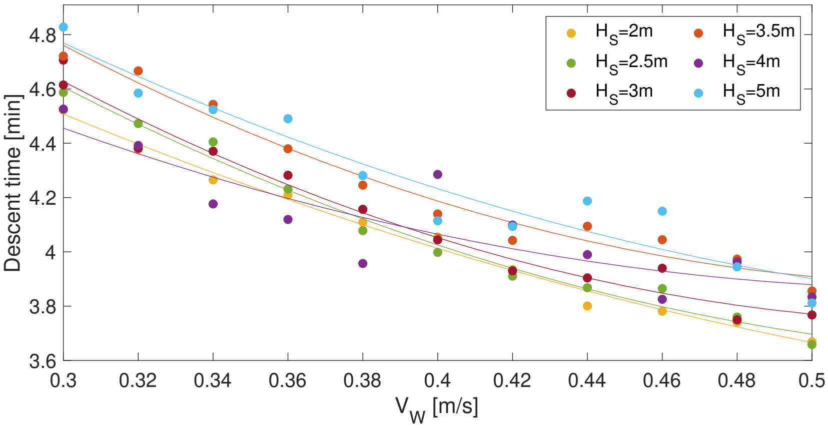

Figure 20: Descent time as a function of winch velocity.

specific wave height. Comparing each of the panels, it is possible to see that, thanks to the heave compensation used in the winch, there are no significant wave-induced differences.

The drift of the anchor on the X and Y positions is explored in Figure 22. It can be seen that the anchor lands further away in the Y direction as wave height increases by up to 12 m. In the X direction, however, the drift is minor, up to 2 m from the starting position.

Figure 23 shows the 3D trajectories of the anchor's descent at all winch velocities and for all wave heights. In comparison with Figure 22, the drift on the direction of the waves (Y) with wave height is not as evident in the 3D trajectories. However, the spread in the X direction with higher waves is evident. Closer to the surface is when the anchor is most influenced by the wave motions. The anchor appears to make circles in the XY plane, which in turn impact the vertical position of the anchor as seen in Figure 14.

The orientation of the anchor for all wave cases is shown in Figure 24. Looking at the yaw angle range, it seems that the anchor turns around it's vertical axis no more than 30° at the highest winch velocities. This value decreases for the slower winch velocities. Pitch shows a working range between 5° and 20° with waves. In contrast, roll has a working range between 1° and 5°.

The speed at which the anchor descend is compared against the winch velocity used. Figure 25 shows the comparison between the different wave heights, including the base case at $H_S = 1$ m.

Figure 26 shows the force range acting on the winch. This range is similar for all wave heights and doesn't not present a trend associated tot eh winch speed. It was an average of 22 kN with maximum and minimum values of 32 and 12 kN, respectively.

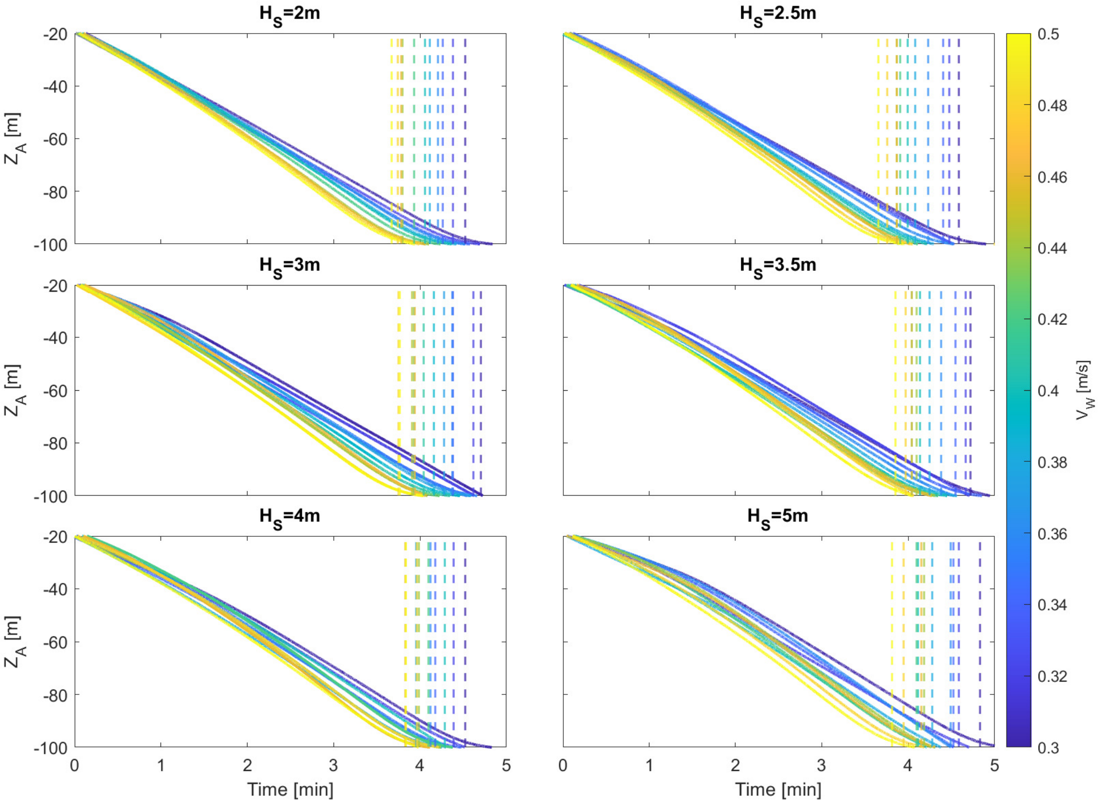

Figure 21: Variation of the anchor's vertical position with time for all wave cases.

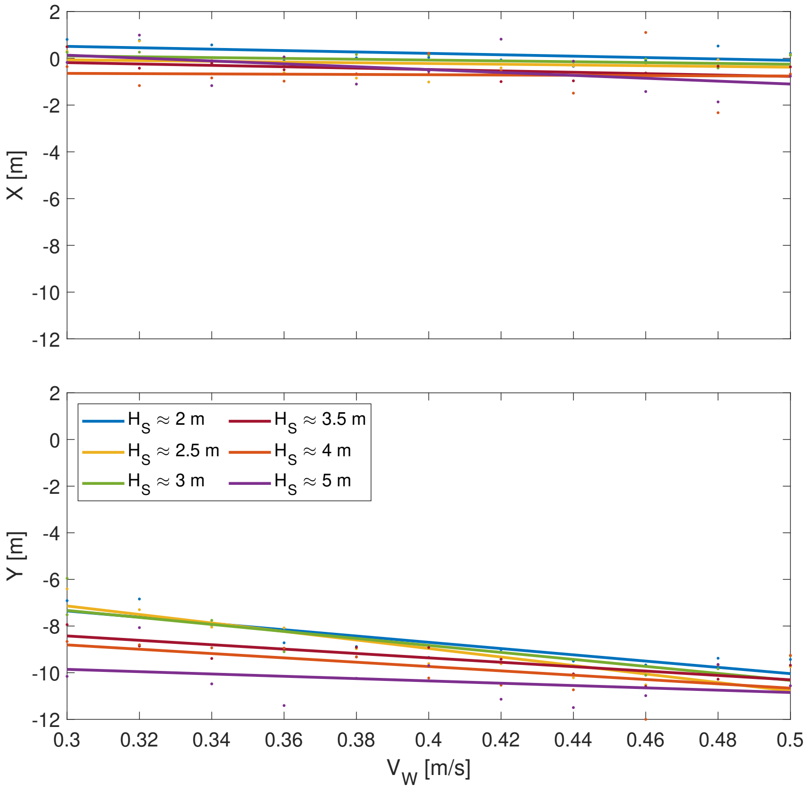

Figure 22: Anchor landing position in (a) X and (b) Y position for all winch speeds and all wave heights.

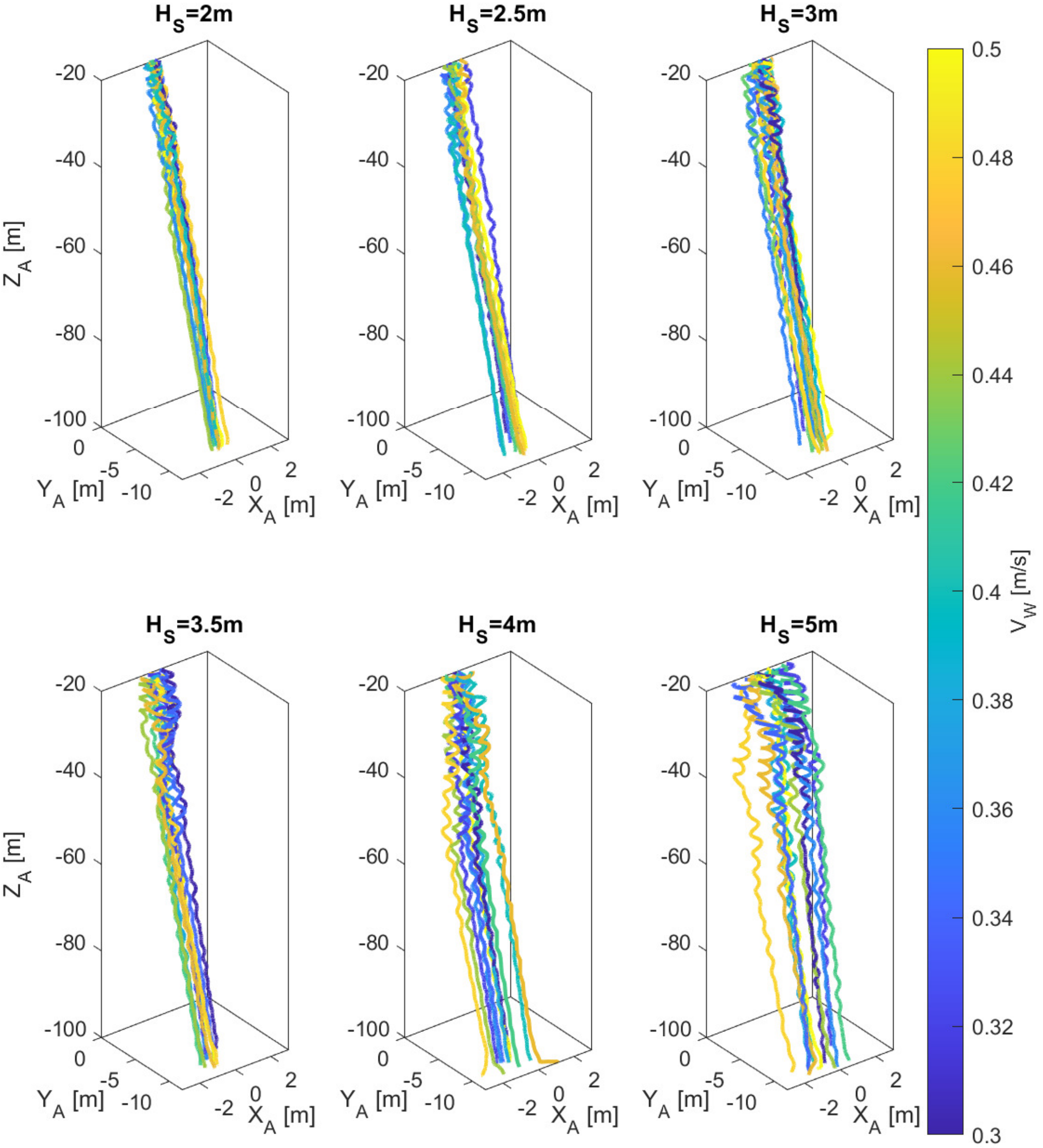

Figure 23: 3D anchor trajectories for all wave cases.

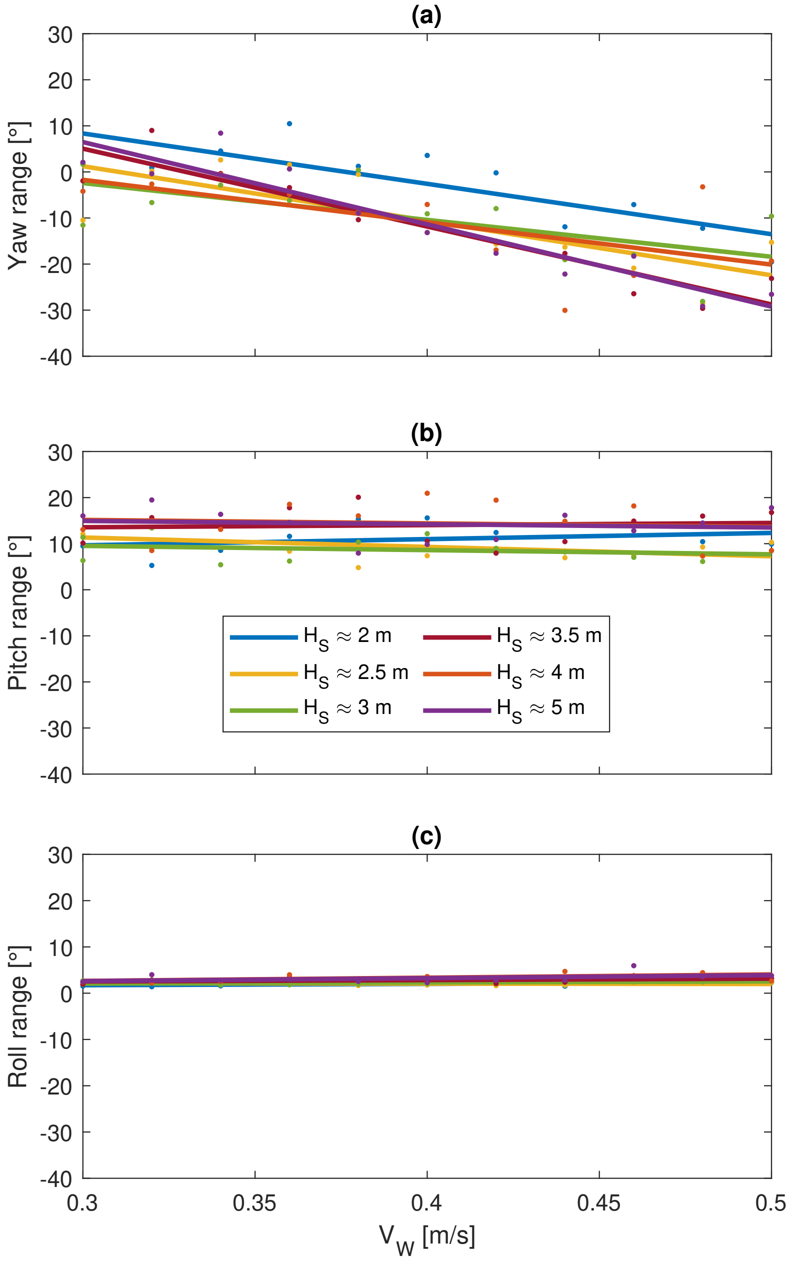

Figure 24: Ranges of angular displacements of the anchor in yaw, pitch and roll directions.

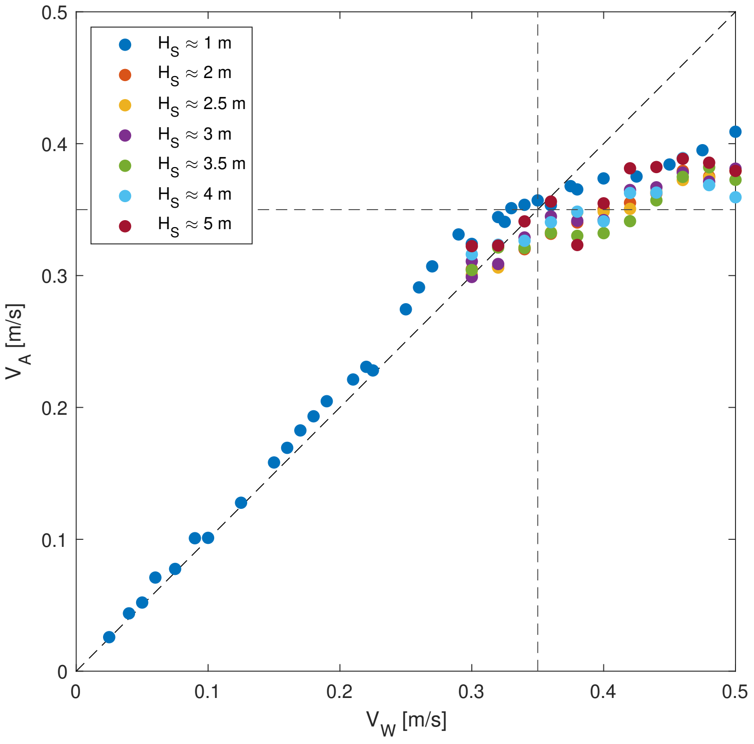

Figure 25: Variation of the anchor deployment speed (V_A) with the winch speed (V_W).

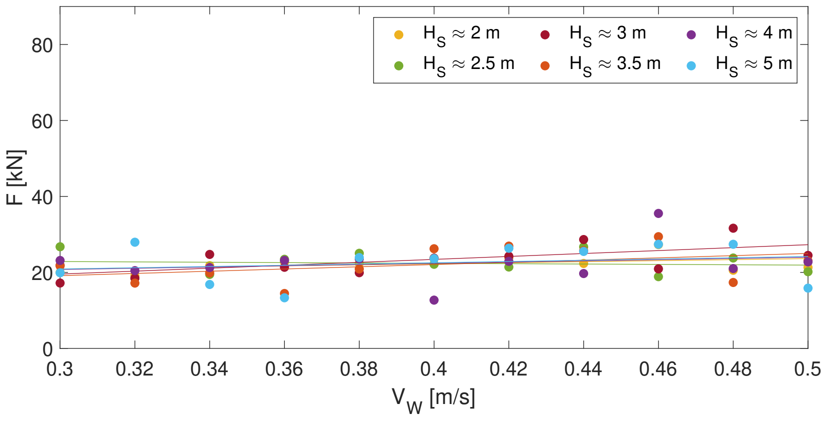

Figure 26: Winch force range as a function of winch velocity.

4.5 Descent - Effects of ocean currents

Once the effect of wave height is explored, the effect of water flows have on the anchor's descent is analysed. Four different anchor weights are tested in parallel with different current velocities. These parameters can be seen in Table 6.

Table 6: Descent parameters

Case	Current [kn]	W$_A$ [t]
1	0.00	6.3
2	0.09	6.3
3	0.18	6.3
4	0.27	6.3
5	0.38	6.3
6	0.49	6.3
7	0.58	6.3
8	0.69	6.3
9	0.76	6.3
10	0.83	6.3
11	0.90	6.3
12	1.01	6.3
12	0.00	12.6
14	0.09	12.6
15	0.18	12.6
16	0.27	12.6
17	0.38	12.6
18	0.49	12.6
19	0.58	12.6
20	0.69	12.6
21	0.83	12.6
22	0.94	12.6
23	1.01	12.6
24	0.00	25.2
25	0.09	25.2
26	0.18	25.2
27	0.27	25.2
28	0.38	25.2
29	0.49	25.2
30	0.58	25.2
31	0.69	25.2
32	0.83	25.2
33	0.90	25.2
34	1.01	25.2
35	0.00	31.5
36	0.09	31.5
37	0.18	31.5
38	0.27	31.5
39	0.49	31.5
40	0.58	31.5
41	0.69	31.5
42	0.83	31.5
43	0.90	31.5
44	1.01	31.5

For the analysis to be accurate, the drag and lift force coefficients used in the simulator have to be calibrated. Calibration was achieved in two steps: 1) drag and lift forces calculation using ANSYS. 2) Drag and lift force coefficients calibrated in simulator by matching the observed forces in the simulator with the force results from step 1. Figure 27 shows these steps. Good agreement is achieved and shown in Figure 27b.

With the drag and lift force coefficients calibrated, the simulations are run with of flow velocities ranging from 0 to 1 kn. In this stage, the effects of the anchor's weight is also investigated. Ballast weight ranges from 6.3 tonnes to 31.5 tonnes.

Results using more ballast are shown in Figures 28 and 29. It appears that all weights take the same amount of time (4 minutes) to descend. However, this is explained looking at the winch force time series, where the tension in the cable increases with weight and the wave-induced oscillations are more visible. These oscillations have the same amplitude for all ballast weights. This means that for each anchor weight, there will be a case-specific winch speed at which descent speed and winch speed are the same (Figure 17).

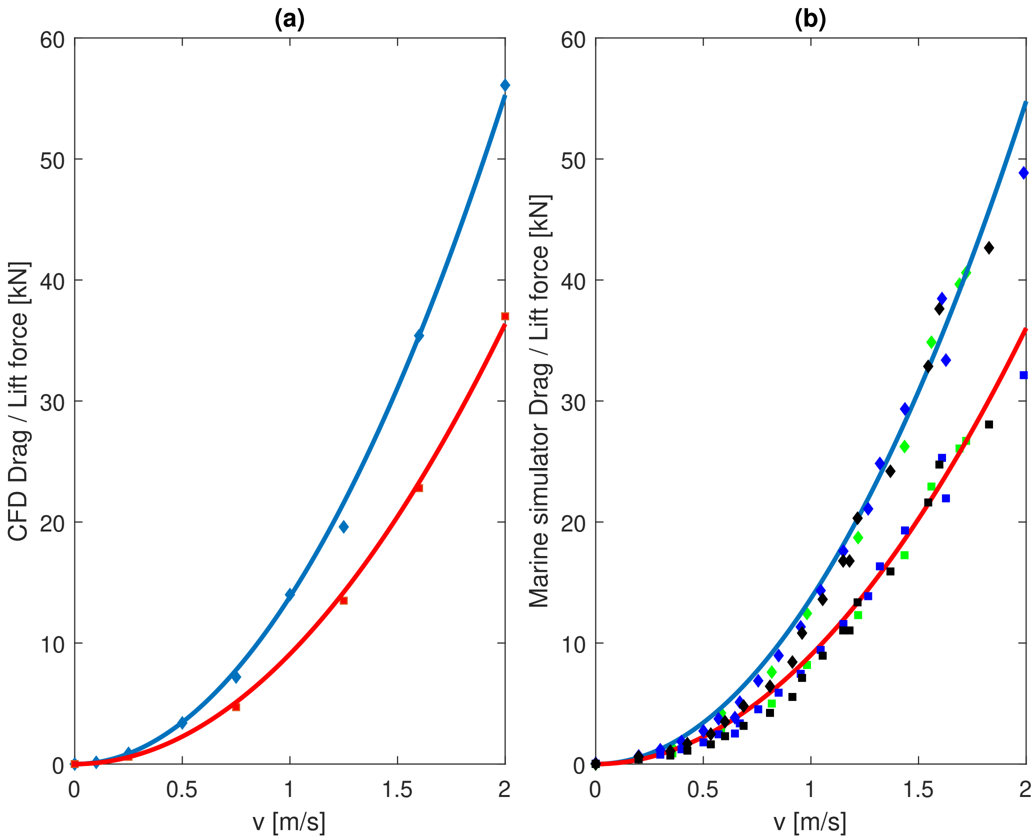

Figure 27: (a) Drag and lift forces as a function of flow velocity from CFD analysis, (b) Calibrated response for drag and lift forces obtained from developed simulation for tow line lengths of $L_{tow} = 22.1$ m (green markers), $L_{tow} = 41.6$ m (blue markers) and $L_{tow} = 60.2$ m (black markers).

Figures 30 to 33 show the 3D trajectories of the anchor at all flow velocities U from the point the winch is released. Each figure is for a specific ballast weight. The X and Y data is normalised to the initial position. At faster currents, the anchor drifts further away from the initial position. With lower flows, the anchor lands almost exactly at the release position. However, for faster speeds and with the lightest ballast (Figure 30), the anchor lands almost 180 m away from the landing position of the flow direction (Y). In the cross-flow direction (X), the anchor lands around 8 m away form the initial position. Form the figures, it is seen that the drift of the anchor decreases as the anchor weight increases. with the heaviest ballast (Figure 33), the anchor drifts around 150 m less from its initial position than with the lightest ballast (Figure 30).

Figure 34 shows the anchor's position (X, Y and Z) and orientation (yaw, pitch and roll) prior to releasing the winch. Similarly, Figure 35 shows the anchor's position and orientation at the time of landing. In both figures, the X and Y data is normalised to the initial position, hence both figures starting at 0.

Similar results can be seen in the 3D trajectory figures. In this case, however, the rate at which the anchor drifts in the Y direction with the flow velocity and the different ballast weights can be quantified. The quadratic equations for the fit are:

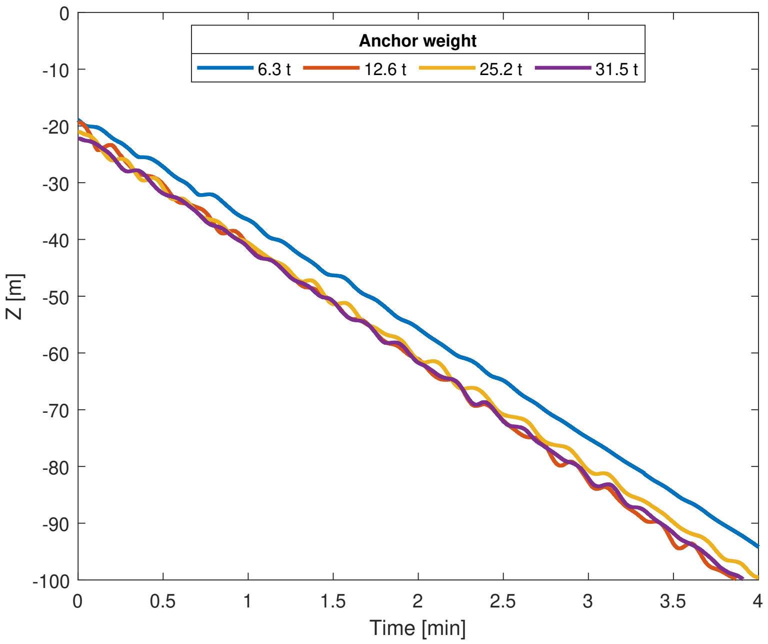

Figure 28: Vertical position of anchors with different ballast weights.

$$y_{6.3t} = -90.1x^2 - 106x - 1.1 \tag{4}$$

$$y_{12.6t} = -75x^2 - 39.8x - 0.6 \tag{5}$$

$$y_{25.2t} = -50x^2 - 12.1x - 0.3 \tag{6}$$

$$y_{31.5t} = -35.1x^2 - 4.8x - 0.7 \tag{7}$$

Due to the close proximity between the data and the quadratic fit, it would be possible to extrapolate the data for faster flows and potentially to different anchor weights.

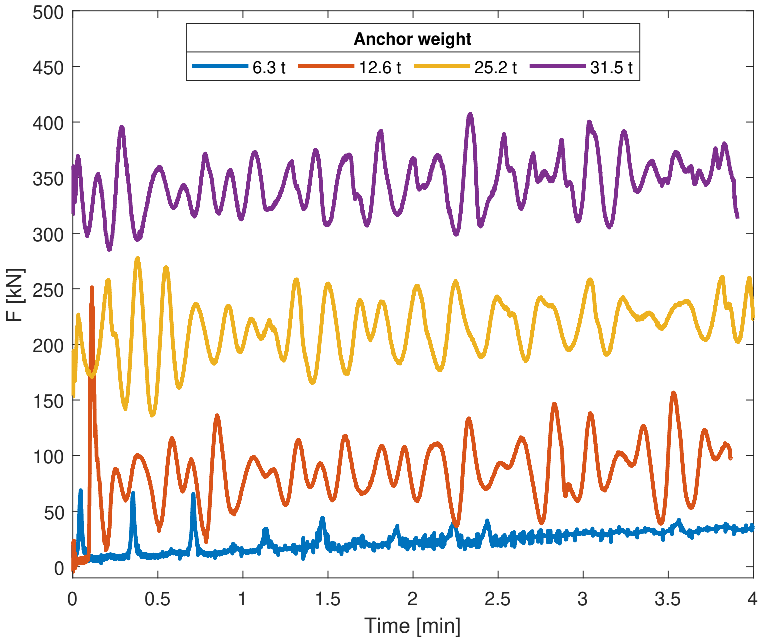

Figure 29: Winch force (F_W) for different anchor ballast weights.

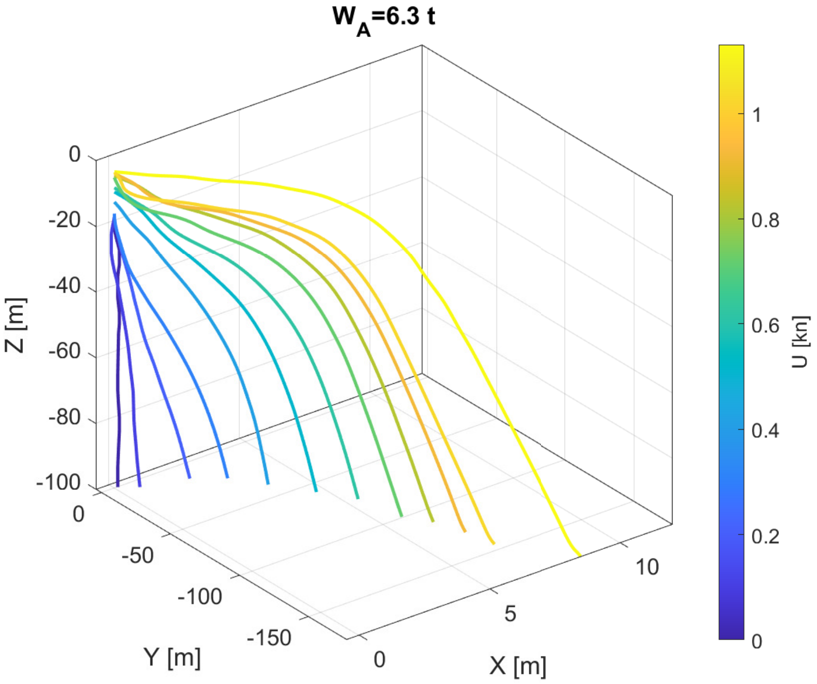

Figure 30: 3D trajectories of anchor descent with a weight of 6.3 tonnes for all current velocities.

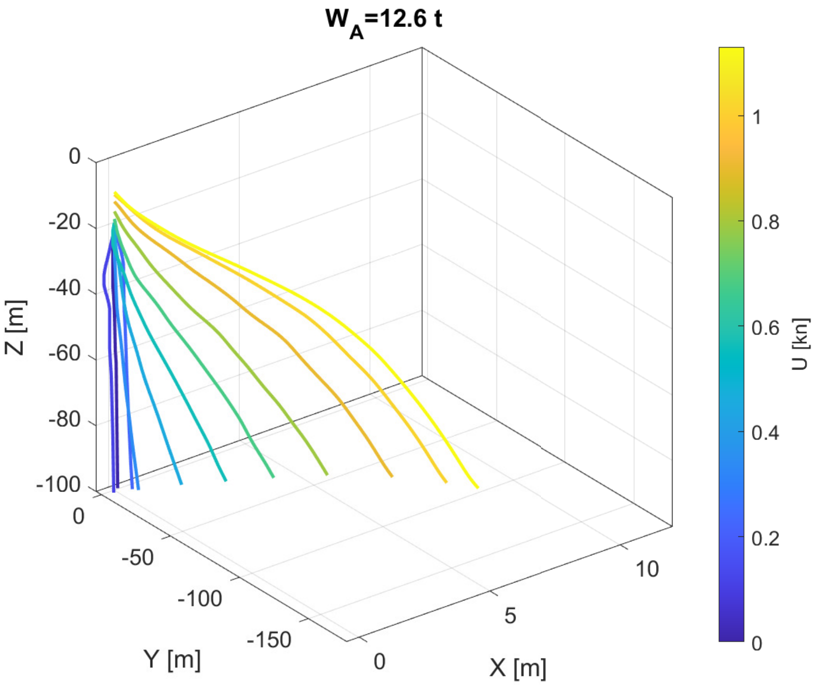

Figure 31: 3D trajectories of anchor descent with a weight of 12.6 tonnes for all current velocities.

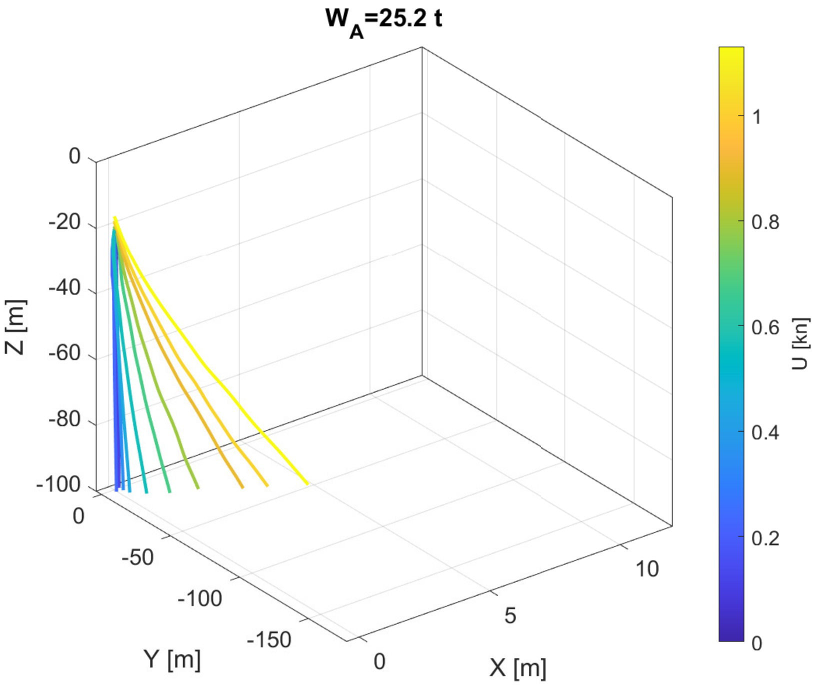

Figure 32: 3D trajectories of anchor descent with a weight of 25.2 tonnes for all current velocities.

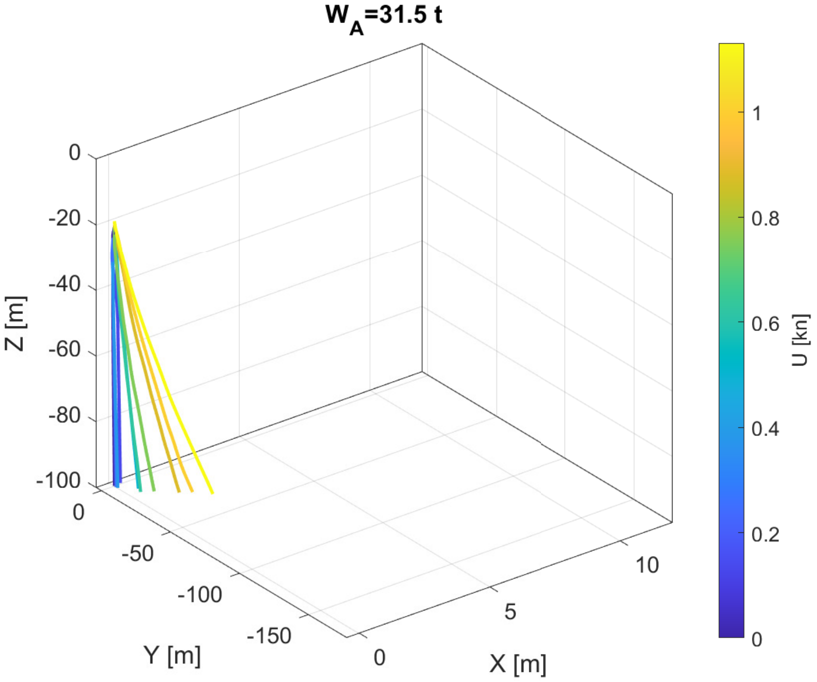

Figure 33: 3D trajectories of anchor descent with a weight of 31.5 tonnes for all current velocities.

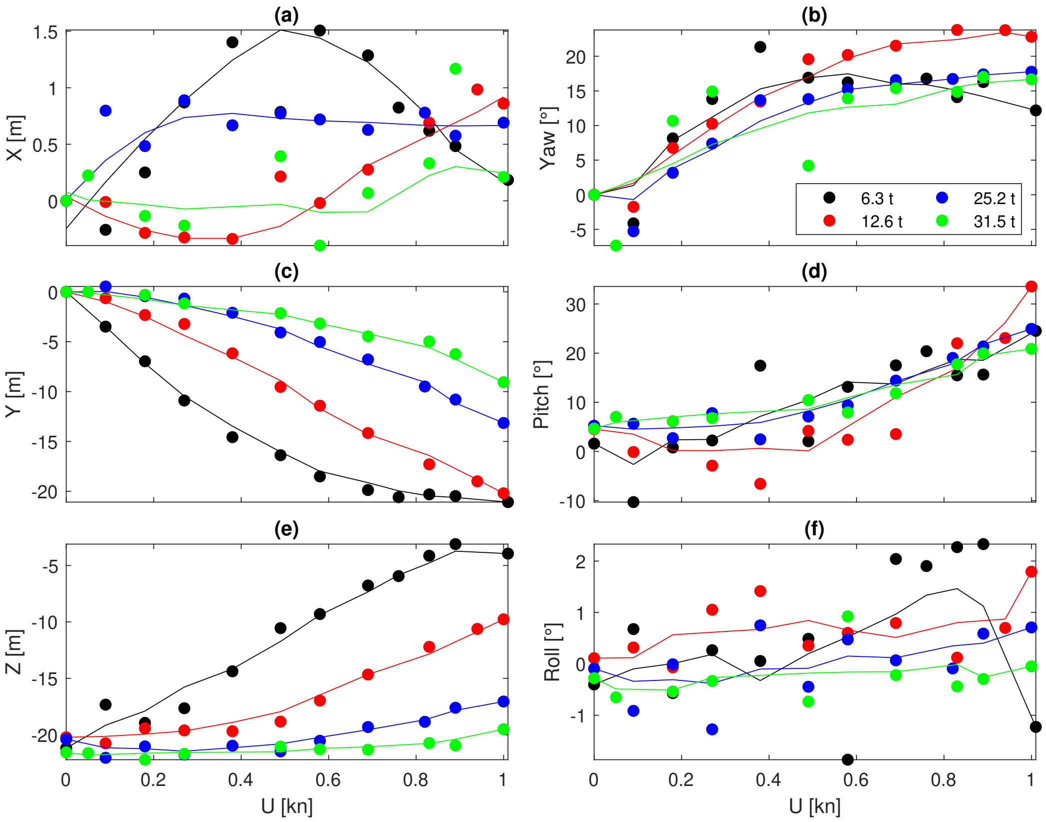

Figure 34: Left column: Variation of the anchor's position (Y, X and Z) before releasing thew winch with U. Right column: Variation of the anchor's orientation (yaw, pitch and roll) before releasing the winch with U

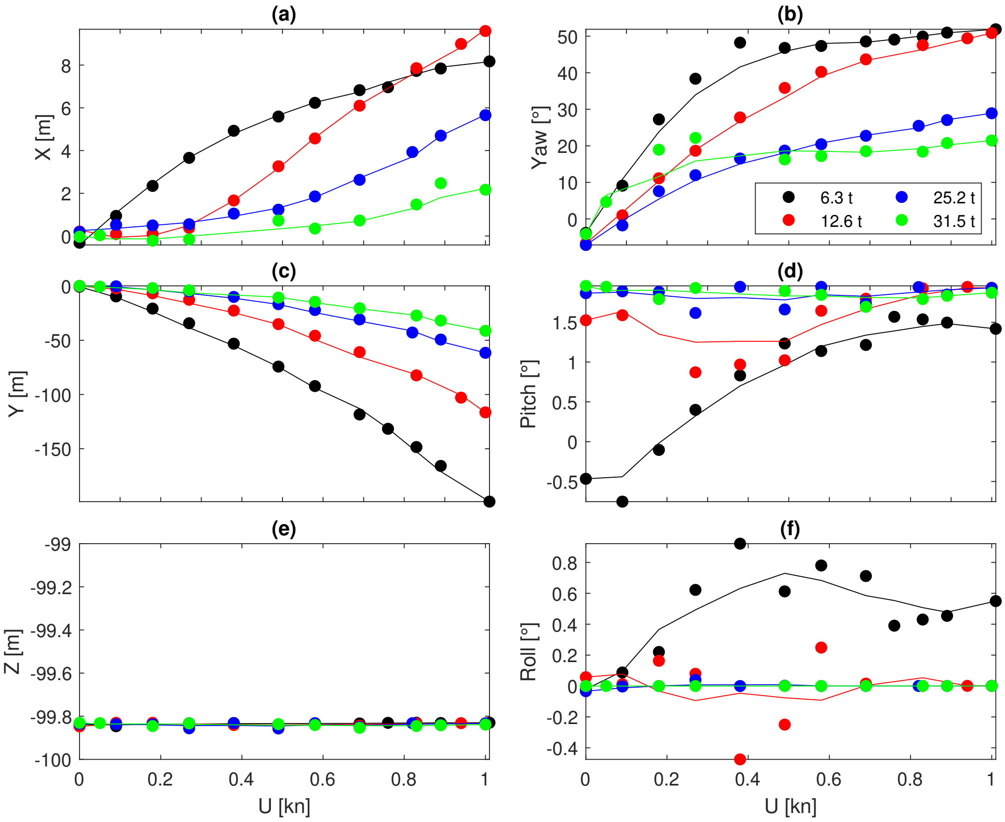

Figure 35: Left column: Variation of the anchor's position (Y, X and Z) at landing with U. Right column: Variation of the anchor's orientation (yaw, pitch and roll) at landing with U

5 Crane deployment

In this section, the deployment of the variable buoyancy anchor is also explored with the use of a heavy lifting crane and compared with the deployment of suction anchors using the same crane. Table 7 shows the significant wave height H_S values used in the simulations for the suction and the variable buoyancy anchors. As a test case, we use a model of a suction anchor used at Hywind Scotland floating wind farm [16]. This allows us to investigate in detail how variable buoyancy anchors would behave when deployed using a crane, as well as benchmark the procedure against typical crane deployment of suction anchors. The Hywind suction anchor are shown in Figure 36 (top panel) and its crane deployment is shown in the bottom panel.

Table 7: Anchor deployment parameters

Suction anchor			**Floating anchor**		
Case	**H_S [m]**	**T_P [s]**	**Case**	**H_S [m]**	**T_P [s]**
1	0.00	10	13	0.00	10
2	0.36	10	14	0.36	10
3	0.80	10	15	0.51	10
4	1.31	10	16	0.80	10
5	1.74	10	17	1.02	10
6	2.11	10	18	1.31	10
7	2.61	10	19	1.52	10
8	2.98	10	20	1.74	10
9	3.41	10	21	1.96	10
10	3.99	10	22	2.11	10
11	4.43	10	23	2.25	10
12	5.01	10	24	2.61	10
			25	2.76	10
			26	2.98	10
			27	3.19	10
			28	3.41	10
			29	3.70	10
			30	3.99	10
			31	4.21	10
			32	4.72	10
			33	5.01	10

The Hywind project utilised 15 suction anchors, with height of 16 m, diameter of 5 m and air mass of 300 t [16]. For the purpose of simulation, we've built a scenario that utilises Polar Onyx [17] vessel model from Simulator library (similar in size and class to Technip FMC Deep Explorer vessel [18] used in actual deployment), which is fixed in X, Y and φ_Z directions and free to move otherwise (heave, pitch, roll). On its back deck we install an NOV 400t (from Simulator library) that will be used to study the deployment of both anchors. The schematics, showing basic setup of both scenarios: crane deployment of variable buoyancy anchor and suction anchor, are shown in Figure 37.

For both cases the crane is kept in the same geometry configuration, with an anchor attached to its hook. In order to establish the effect of waves on the crane deployment scenario for both anchors, we set the crane winch speed to the same value ($v_W = 0.35\,\frac{\mathrm{m}}{\mathrm{s}}$) and vary the significant wave height, H_S (within range 0-5 m). As in previous tests, we use the JONSWAP wave spectrum, with wave period of 10 s to generate irregular waves. For both cases, the deployment process consists of initial stage in which the anchor is suspended on the crane and oscillates above the water surface. The anchors are kept in this stage sufficiently long to allow for steady state solution to be reached. The purpose of this is to allow us to quantify maximum displacements each anchor can reach subject to wave loading passed through the vessel. Next the deployment stage starts, where we monitor anchors descent through the splash zone, until it reaches the seabed (100 m depth).

5.1 Suction anchors

In Figures 38-41, we depict examples of family of time histories of crane winch force F, angular displacements φ_X, φ_Y, φ_Z and displacements X, Y, Z of the suction anchor for wave heights of: 0.8 m, 1.74 m, 2.61 m, 3.99 m, respectively. Note, that time histories shown in blue correspond to the initial stage, when the anchor is suspended under the crane hook (pre-deployment). Time histories shown in orange colour, depict the deployment stage, from the moment the crane winch is enabled. In this way we can establish the maximum amplitudes of vibrations observed for all degrees-of-freedom for the suction anchor. The general trend for the suction anchor, is that the maximum amplitudes are observed in the initial stage and as we pass through the splash zone and further down to the seabed, the level of vibrations diminishes. The main stages of the operation are visible on the graphs in Figures 38-41, which are the moment the winch is enabled (spike in the force signal) and reaching the seabed (force goes to zero, no change in axial position of the anchor). Interestingly, in some cases (as in Figure 41), we observe a bounce back once the anchor hits the seabed, which results in rapid change of force. The reason for this behaviour is the interaction between vessel, that heaves on waves and the cable that connects it to the anchor. Similar behaviour has been observed when deploying variable buoyancy anchors using the winch (See Section 4).

In Figures 42-44, we present 3D trajectories of the suction anchor for both initial and deployment stages under different environmental conditions, H_S : 0.36, 0.80, 1.31, 1.74, 2.11, 2.61, 2.98, 3.41, 3.99 and 5.01 m, respectively. The surface marked in cyan colour denotes the water level, while the blue and orange colours mark the initial and deployment stages, respectively (as before). These trajectories allow us to visualise the level of vibrations experienced by the suction anchor in each stage. The level of vibrations increases with significant wave height, H_S.

In Figure 45, we present the mean force in the crane winch (left panel) and the maximum amplitude of the force observed (right panel) as a function of significant wave height, H_S. We see that the mean value remains constant while there is significant changes in the amplitude of the force observed, while the suction anchor is suspended on the crane. We observe a local maxima around $H_S = 0.8$m and $H_S = 2.11$m, after which the force amplitude ΔF keeps increasing. When comparing the maximum amplitudes observed for other degrees-of-freedom, shown in Figure 46, we observe a linear trend for ΔX, ΔY, ΔZ, $\Delta\varphi_X$, $\Delta\varphi_Y$ as the significant wave

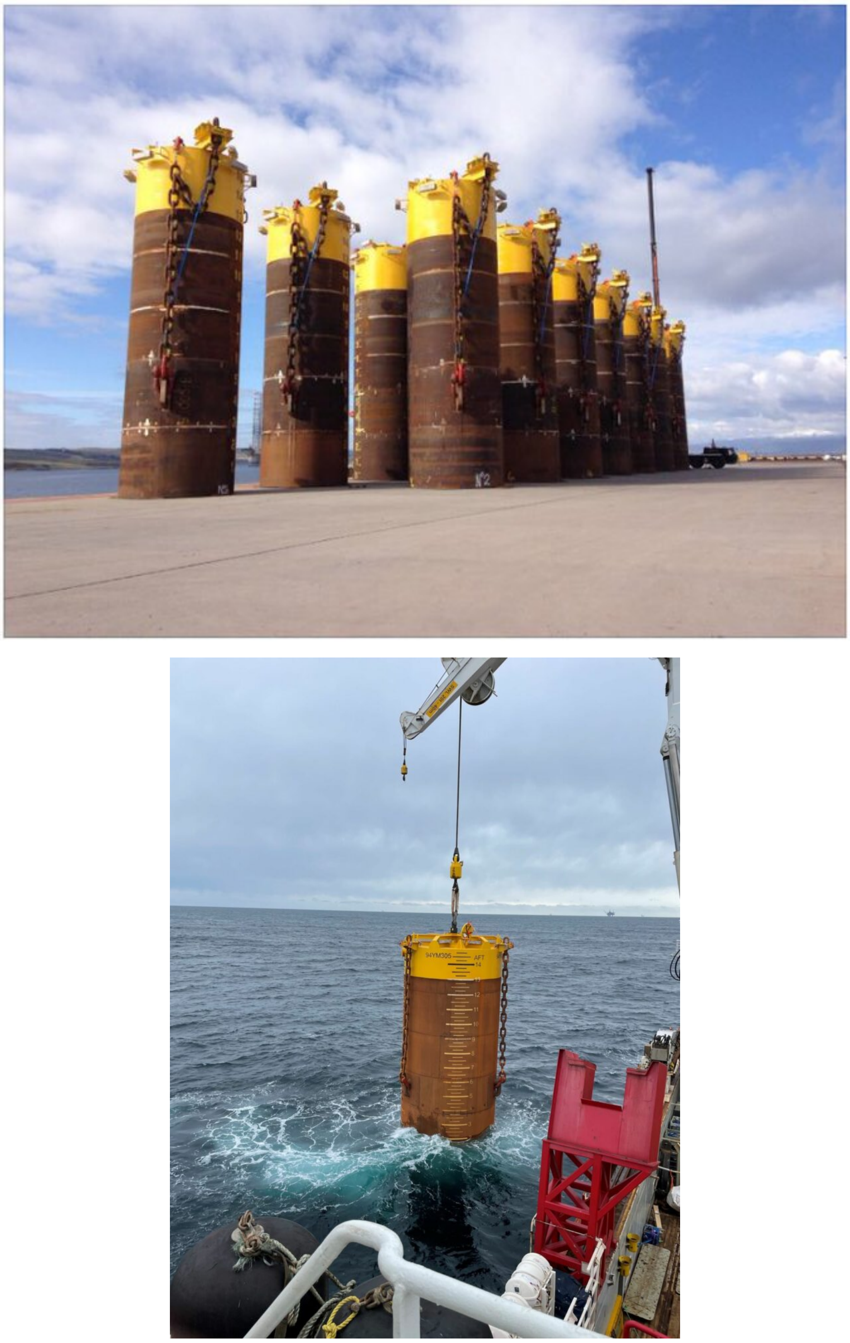

Figure 36: (top panel) Hywind Scotland suction anchors [16]. (bottom panel) Crane installation of Hywind suction anchor [19].

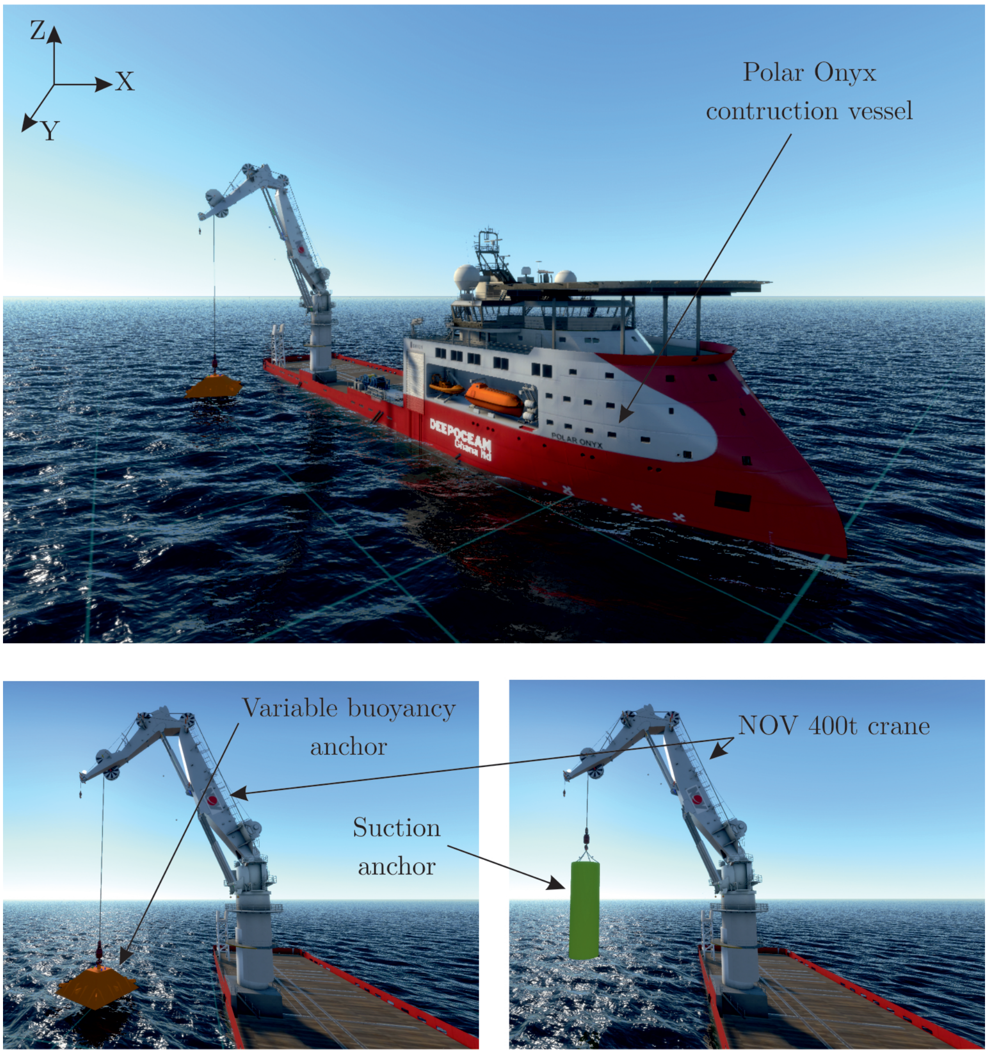

Figure 37: Schematic depicting the setup of the model used to study crane deployment of suction (bottom right panel) and variable buoyancy anchor (bottom left). The model consists of Polar Onyx construction vessel with its X_V, Y_V, φ_{VZ} coordinates fixed, NOV 400t crane placed on back deck of the vessel, and suction/variable buoyancy anchors suspended on the crane hook. The suction anchor has air mass of 300t [20], while the variable buoyancy anchor has air mass of 175t.

height increases. In term of yaw amplitude, we observe a local maximum around $H_S = 1.0$m, followed by very small rotations, which again starts increasing as we pass $H_S = 4$m.

5.2 Variable buoyancy anchor

As for the suction anchor, we conduct a same type of analysis to establish what happens when variable buoyancy anchor is deployed using a crane under varying environmental conditions, wave height in particular. In Figures 47-50, we present example time histories of crane winch force F, angular displacements φ_X, φ_Y, φ_Z and displacements X, Y, Z of the variable buoyancy anchor for wave heights of: 0.8 m, 1.74 m, 2.61 m, 3.99 m, respectively. Note, that time histories shown in blue correspond to the initial stage, when the anchor is suspended under the crane hook (pre-deployment). Time histories shown in orange colour, depict the deployment stage, from the moment the crane winch is enabled.

The behaviour of the variable buoyancy is similar to that of the suction anchor, in terms of the fact that maximum vibrations occur in the initial stage when the anchor is suspended on the crane and gets mitigated as the anchor passes through the splash zone in the deployment stage. One clear difference is related to the fact that once the variable buoyancy anchor gets into water, a significant change in its weight occurs, as shown in the winch force F time histories. This causes the vibrations along X and Y axes dampen much quicker. On the other hand, we observe that in the deployment stage, as the anchor passes through splash zone, significant changes in its yaw angle φ_Z occur. These can be related to the shape of the anchor as well its low weight in water, and therefore amplified loading due to waves. Examples of 3D trajectories of the variable buoyancy anchor are shown in Figures 51-53 for both initial and deployment stages under different environmental conditions, H_S : 0.36, 0.80, 1.31, 1.74, 2.11, 2.61, 2.98, 3.41, 3.99, 4.43, 4.72 and 5.01 m, respectively. We can observe increased footprint (max X and Y) of the variable anchor as it is suspended on the crane. The comparison between the variable buoyancy anchor and the suction anchor in this respect is shown in Figure 56, where we plot an ellipse for each wave height, which major and minor axes correspond to maximum amplitude in X and Y observed in each case.

In Figure 55, we show how the mean winch force and its amplitude) change with wave height. The trend is similar to that observed for suction anchor, but we see a linear relationship between ΔF and H_S. As before, we observe a linear trend for ΔX, ΔY, ΔZ, $\Delta\varphi_X$, $\Delta\varphi_Y$ as the significant wave height increases. In term of yaw amplitude, we observe a local maximum around $H_S = 2.0$m, followed by local minimum around $H_S = 3.0$m , which again starts increasing as we pass $H_S = 3$m.

Interestingly, if we compare the yaw angle induced as both anchor descends to the seabed, shown in Figure 57, we observe that suction anchor will have a local maximum around $H_S = 1.0\,$m, while the variable buoyancy anchor has local maximum around $H_S = 0.8\,$m, though roughly 3 times that of the suction anchor. As H_S increases the amplitude of yaw for variable buoyancy anchor remains roughly constant from $H_S = 1.0\,$m to $H_S = 5.0\,$m. For suction anchor the situation is slightly different, as the results indicate another local maximum around $H_S = 4.8\,$m

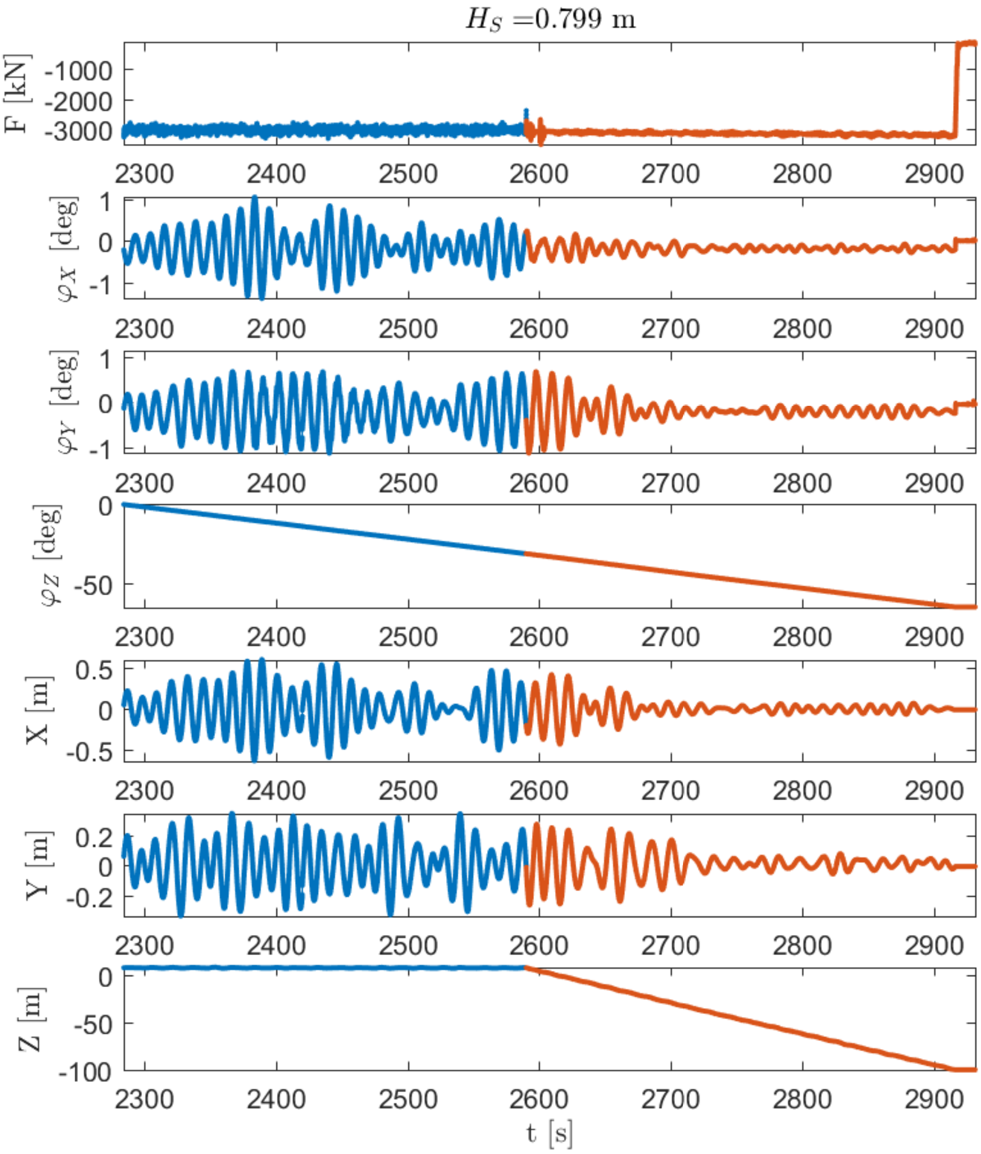

Figure 38: Example time histories for significant wave height of $H_S = 0.80\,\mathrm{m}$ for crane force F, angular displacements (pitch, roll, yaw) of the suction anchor, φ_X, φ_Y, φ_Z and displacements of the variable buoyancy anchor along X, Y, and Z axes, respectively. Note, that time histories shown in blue correspond to anchor hanging on the crane and those shown in orange correspond to deployment stage with crane winch speed of $V_W = 0.35\,\frac{\mathrm{m}}{\mathrm{s}}$.

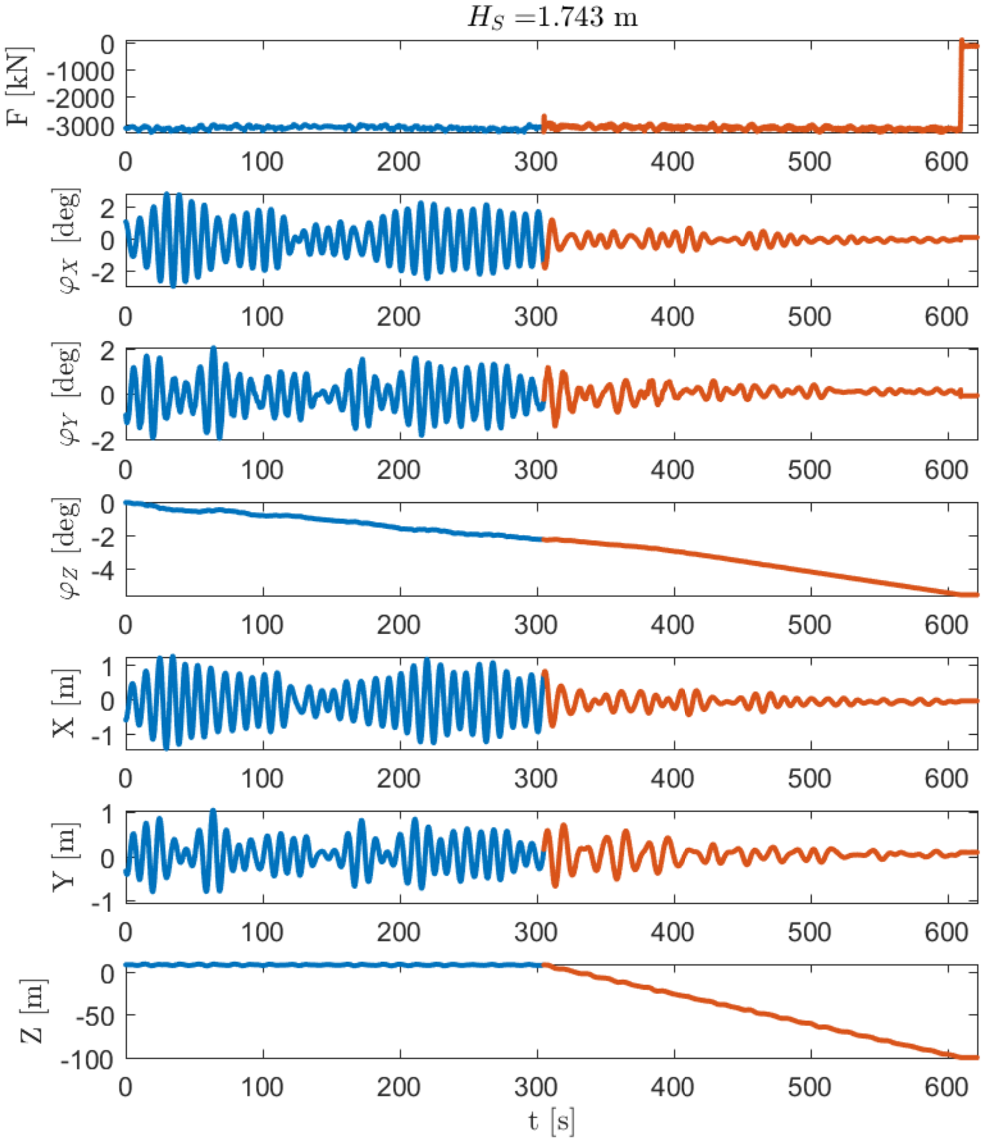

Figure 39: Example time histories for significant wave height of $H_S = 1.74\,\text{m}$ for crane force F, angular displacements (pitch, roll, yaw) of the suction anchor, φ_X, φ_Y, φ_Z and displacements of the variable buoyancy anchor along X, Y, and Z axes, respectively. Note, that time histories shown in blue correspond to anchor hanging on the crane and those shown in orange correspond to deployment stage with crane winch speed of $V_W = 0.35\,\frac{\text{m}}{\text{s}}$.

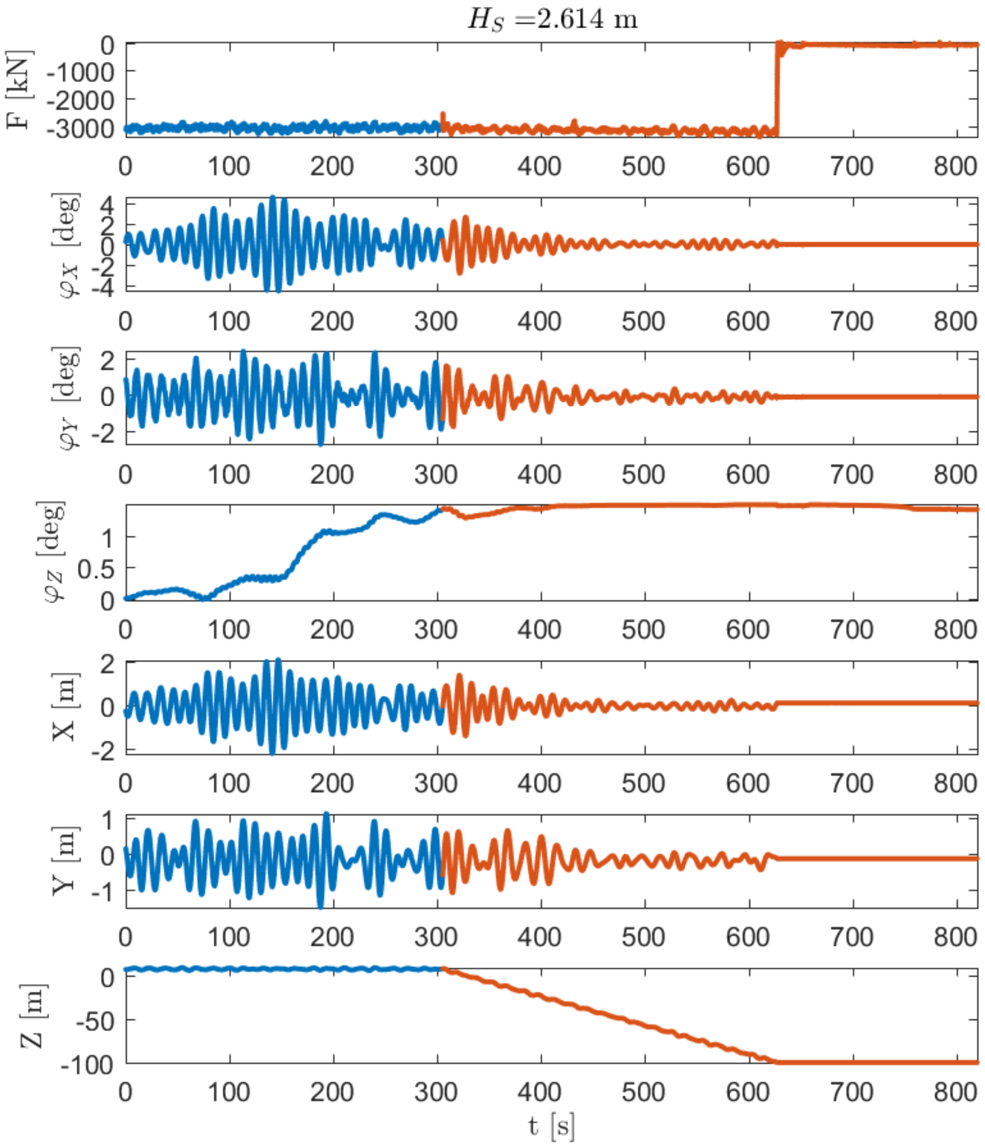

Figure 40: Example time histories for significant wave height of $H_S = 2.61\,\mathrm{m}$ for crane force F, angular displacements (pitch, roll, yaw) of the suction anchor, φ_X, φ_Y, φ_Z and displacements of the variable buoyancy anchor along X, Y, and Z axes, respectively. Note, that time histories shown in blue correspond to anchor hanging on the crane and those shown in orange correspond to deployment stage with crane winch speed of $V_W = 0.35\,\frac{\mathrm{m}}{\mathrm{s}}$.

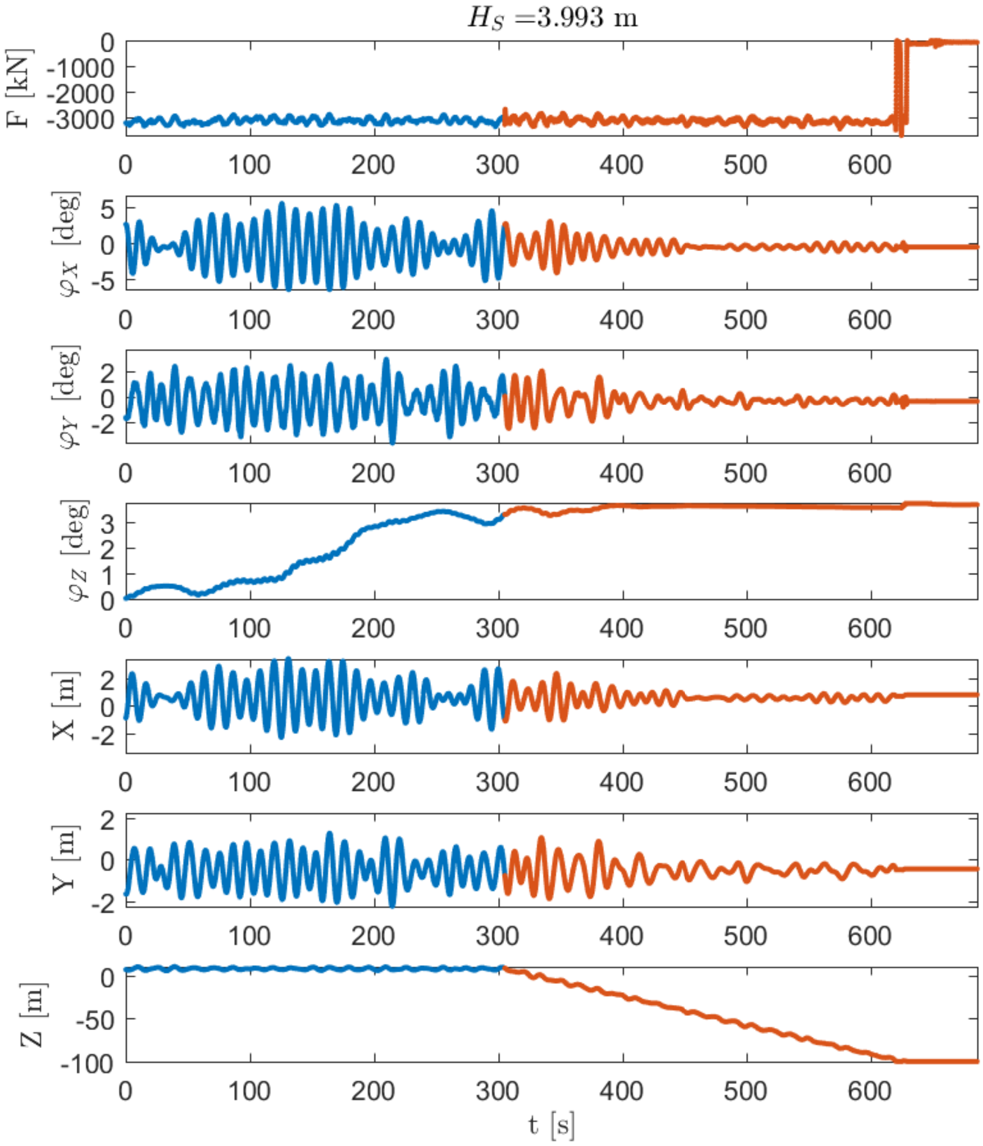

Figure 41: Example time histories for significant wave height of $H_S = 3.99\,\mathrm{m}$ for crane force F, angular displacements (pitch, roll, yaw) of the suction anchor, φ_X, φ_Y, φ_Z and displacements of the variable buoyancy anchor along X, Y, and Z axes, respectively. Note, that time histories shown in blue correspond to anchor hanging on the crane and those shown in orange correspond to deployment stage with crane winch speed of $V_W = 0.35\,\frac{\mathrm{m}}{\mathrm{s}}$.

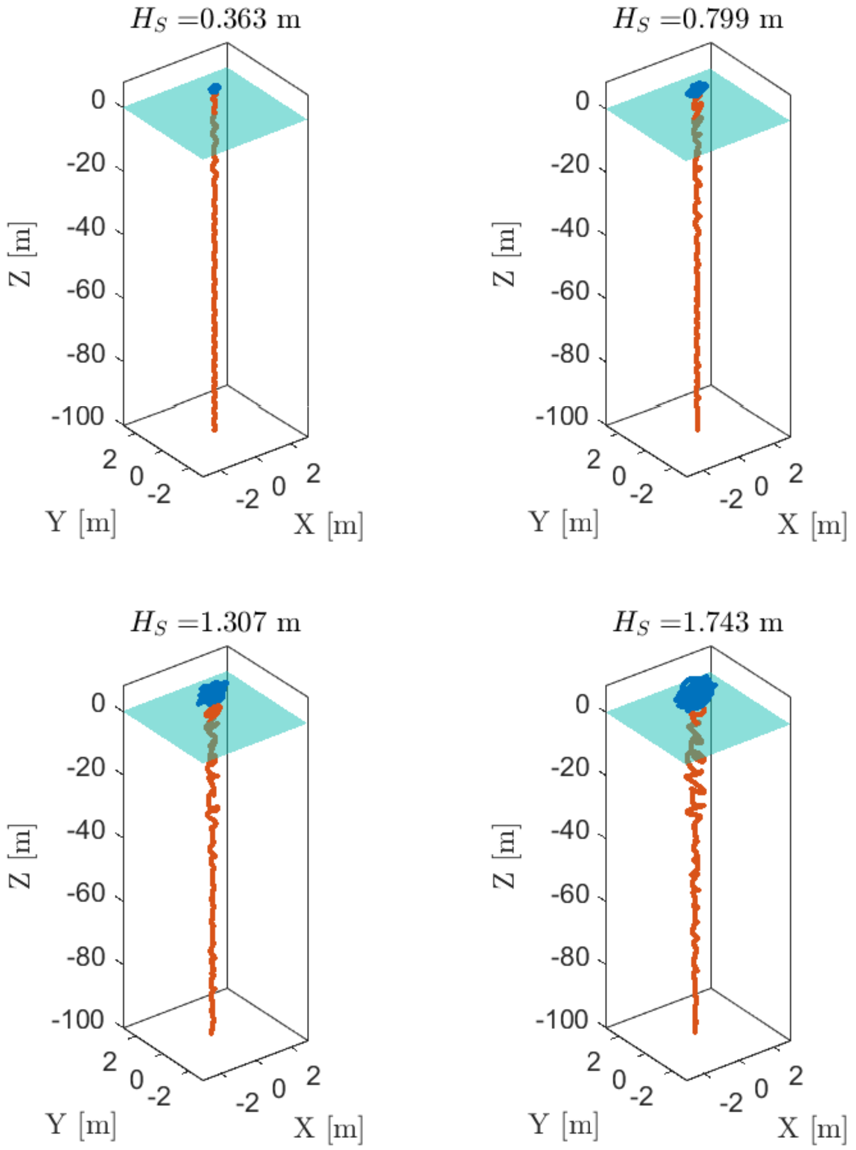

Figure 42: Example 3D trajectories of suction anchor deployed to 100 m water depth under varying significant wave heights: $H_S = 0.36\,\mathrm{m}$, $H_S = 0.79\,\mathrm{m}$, $H_S = 1.31\,\mathrm{m}$, $H_S = 1.74\,\mathrm{m}$, respectively. Note, that trajectories shown in blue correspond to anchor hanging on the crane and those shown in orange correspond to deployment stage with crane winch speed of $V_W = 0.35\,\frac{\mathrm{m}}{\mathrm{s}}$. The plane marked in cyan colour denotes the water surface.

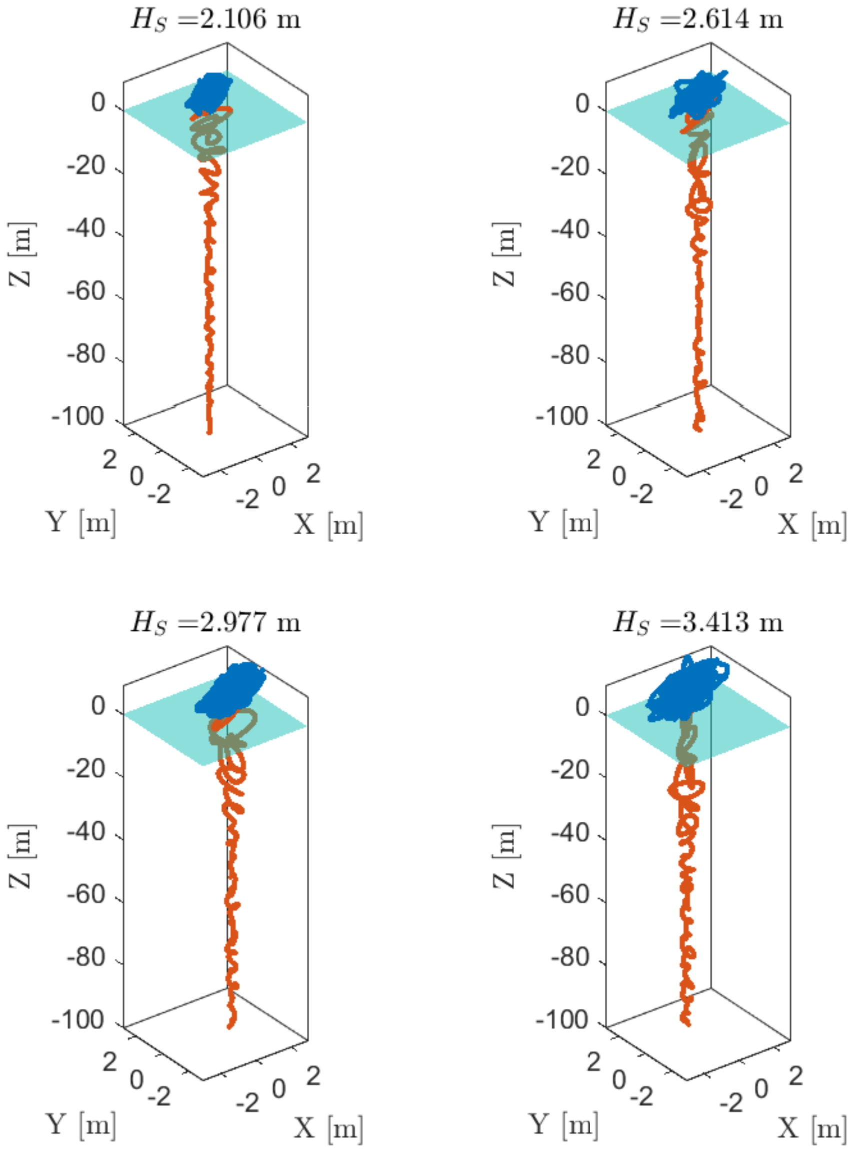

H_S =2.106 m

H_S =2.614 m

H_S =2.977 m

H_S =3.413 m

Figure 43: Example 3D trajectories of suction anchor deployed to 100 m water depth under varying significant wave heights: $H_S = 2.11\,\mathrm{m}$, $H_S = 2.61\,\mathrm{m}$, $H_S = 2.97\,\mathrm{m}$, $H_S = 3.41\,\mathrm{m}$, respectively. Note, that trajectories shown in blue correspond to anchor hanging on the crane and those shown in orange correspond to deployment stage with crane winch speed of $V_W = 0.35\,\frac{\mathrm{m}}{\mathrm{s}}$. The plane marked in cyan colour denotes the water surface.

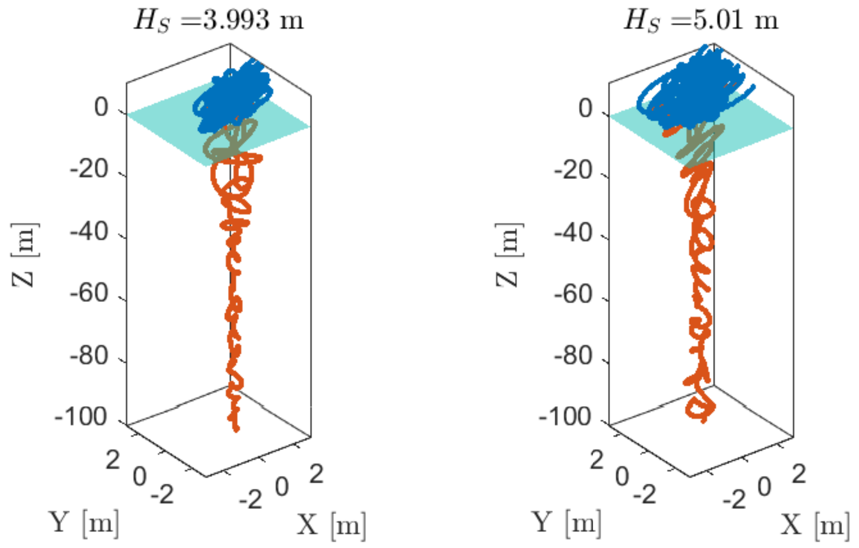

Figure 44: Example 3D trajectories of suction anchor deployed to 100 m water depth under varying significant wave heights: $H_S = 3.99\,\mathrm{m}$, $H_S = 5.01\,\mathrm{m}$, respectively. Note, that trajectories shown in blue correspond to anchor hanging on the crane and those shown in orange correspond to deployment stage with crane winch speed of $V_W = 0.35\,\frac{\mathrm{m}}{\mathrm{s}}$. The plane marked in cyan colour denotes the water surface.

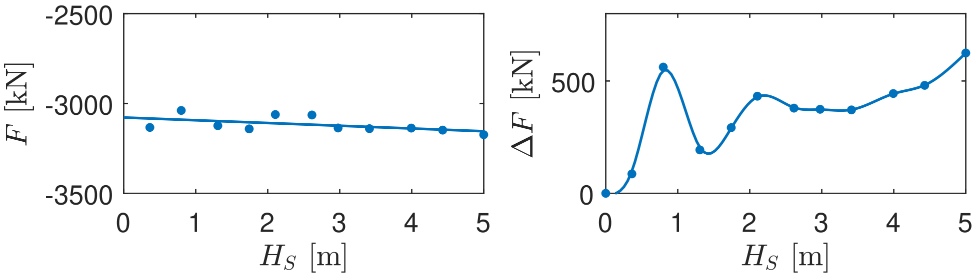

Figure 45: (Left panel) Mean force F observed by the crane winch and (Right panel) peak to peak amplitude ΔF of the winch force F as a function of significant wave height H_S (Suction anchor suspended on the crane, pre-deployment).

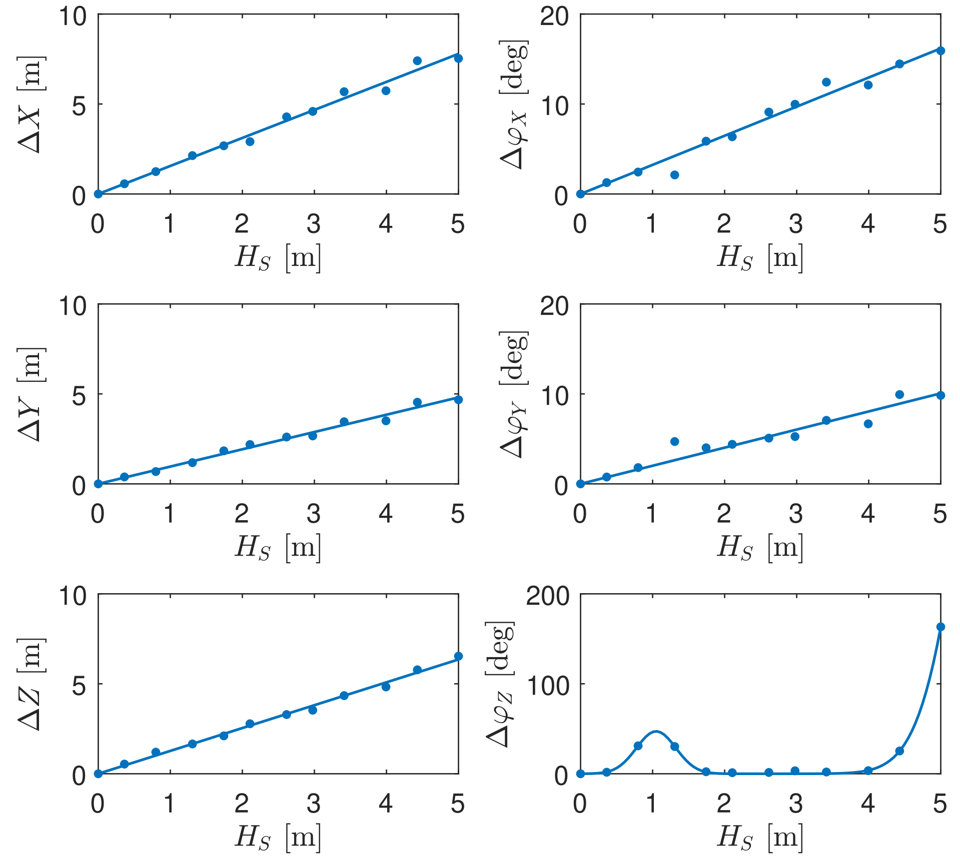

Figure 46: (Left panels) Peak to peak amplitudes of suction anchor displacements, ΔX, ΔY, ΔZ and (Right panels) peak to peak amplitudes of angular displacements (pitch, roll, yaw) of the variable buoyancy anchor, $\Delta \varphi_X$, $\Delta \varphi_Y$, $\Delta \varphi_Z$ as a function of significant wave height H_S (Suction anchor suspended on the crane, pre-deployment).

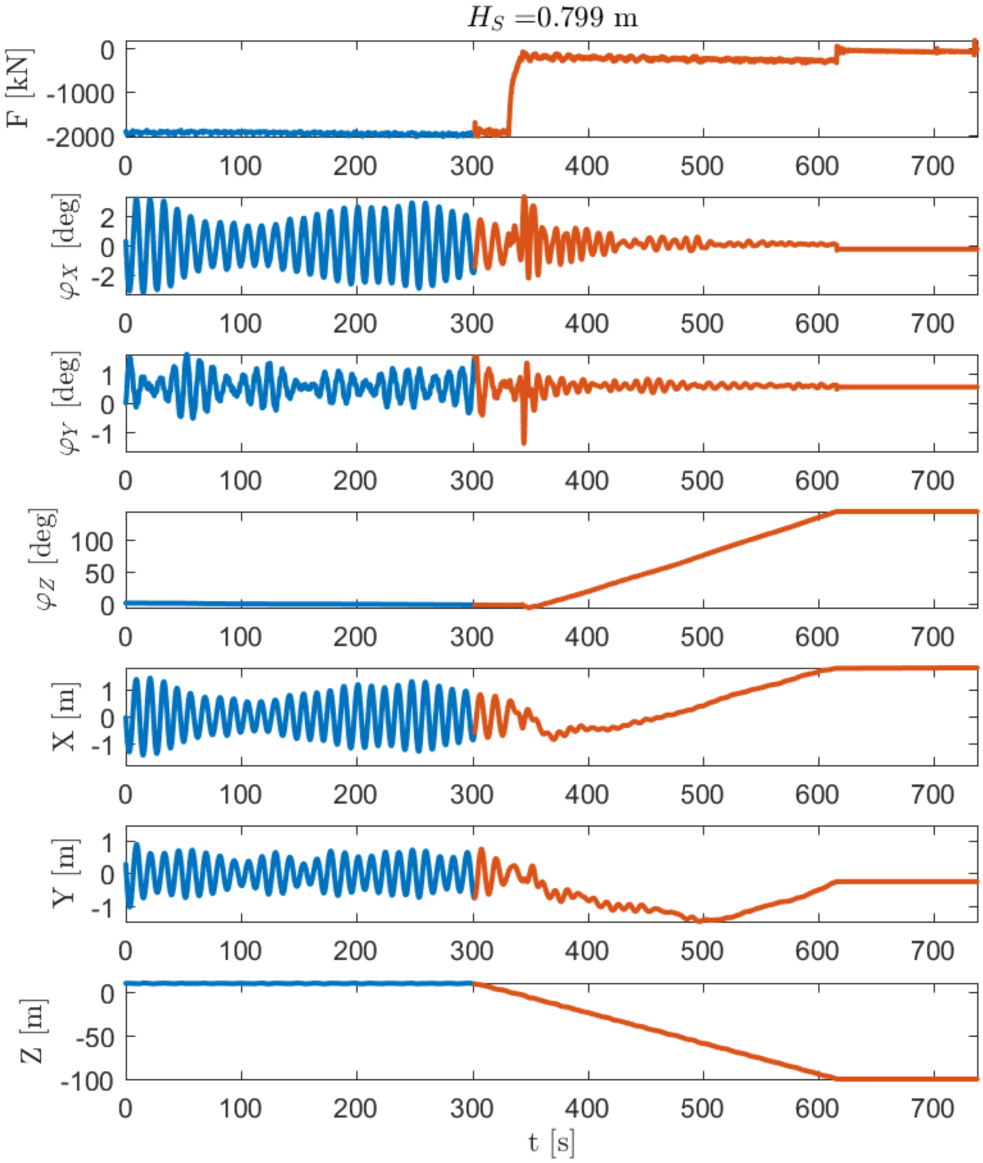

Figure 47: Example time histories for significant wave height of $H_S = 0.80\,\mathrm{m}$ for crane force F, angular displacements (pitch, roll, yaw) of the variable buoyancy anchor, φ_X, φ_Y, φ_Z and displacements of the variable buoyancy anchor along X, Y, and Z axes, respectively. Note, that time histories shown in blue correspond to anchor hanging on the crane and those shown in orange correspond to deployment stage with crane winch speed of $V_W = 0.35\,\frac{\mathrm{m}}{\mathrm{s}}$.

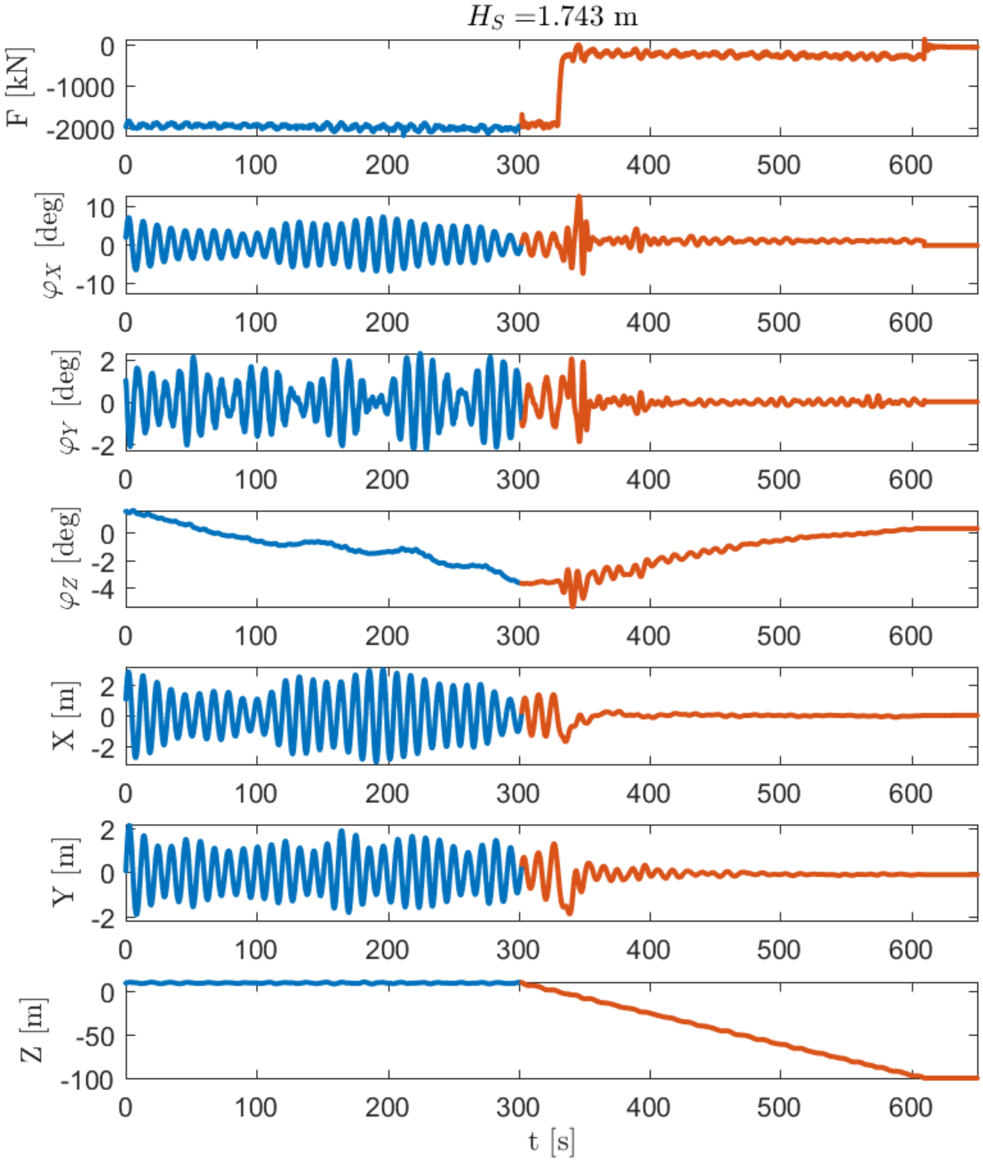

Figure 48: Example time histories for significant wave height of $H_S = 1.74\,\mathrm{m}$ for crane force F, angular displacements (pitch, roll, yaw) of the variable buoyancy anchor, φ_X, φ_Y, φ_Z and displacements of the variable buoyancy anchor along X, Y, and Z axes, respectively. Note, that time histories shown in blue correspond to anchor hanging on the crane and those shown in orange correspond to deployment stage with crane winch speed of $V_W = 0.35\,\frac{\mathrm{m}}{\mathrm{s}}$.

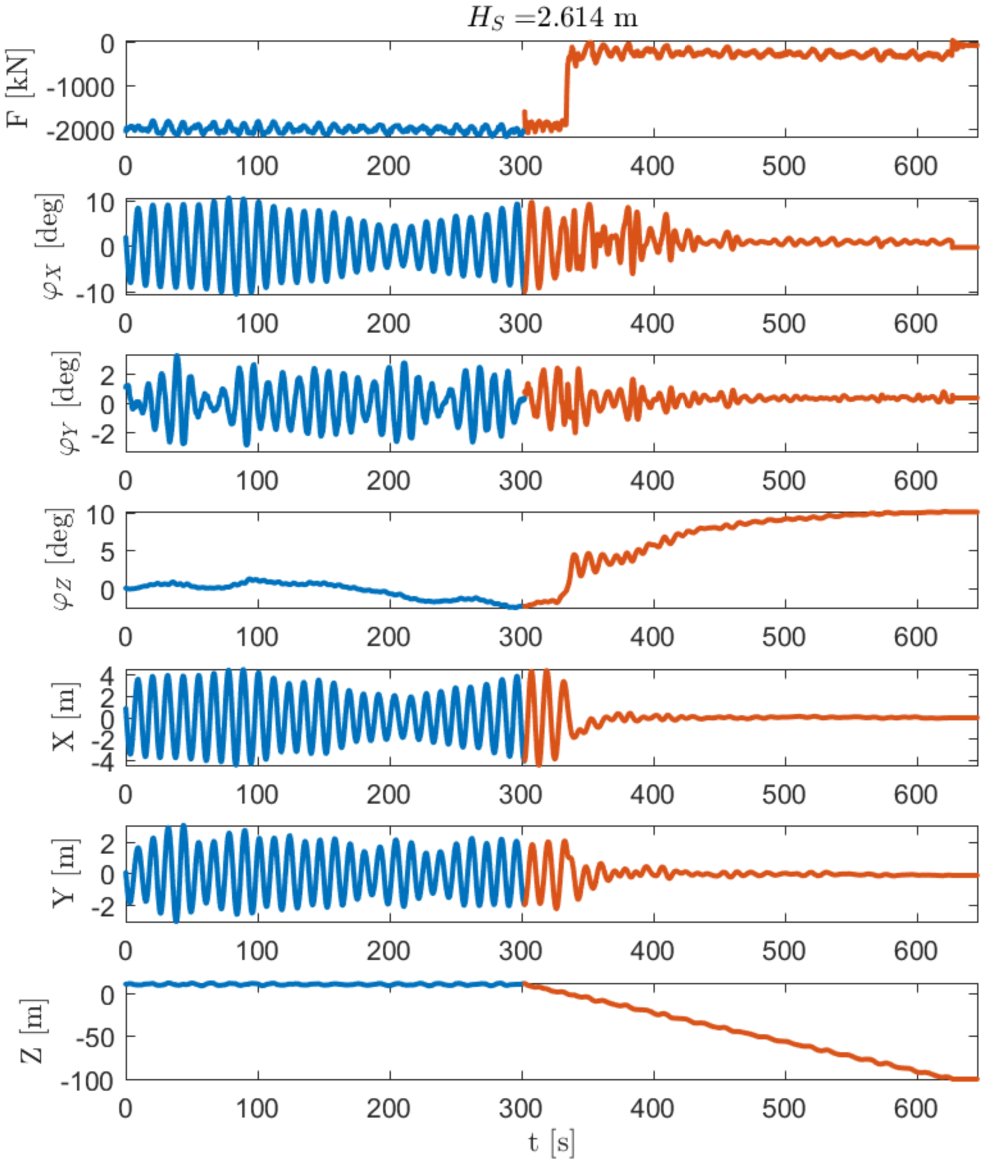

Figure 49: Example time histories for significant wave height of $H_S = 2.61\,\mathrm{m}$ for crane force F, angular displacements (pitch, roll, yaw) of the variable buoyancy anchor, φ_X, φ_Y, φ_Z and displacements of the variable buoyancy anchor along X, Y, and Z axes, respectively. Note, that time histories shown in blue correspond to anchor hanging on the crane and those shown in orange correspond to deployment stage with crane winch speed of $V_W = 0.35\,\frac{\mathrm{m}}{\mathrm{s}}$.

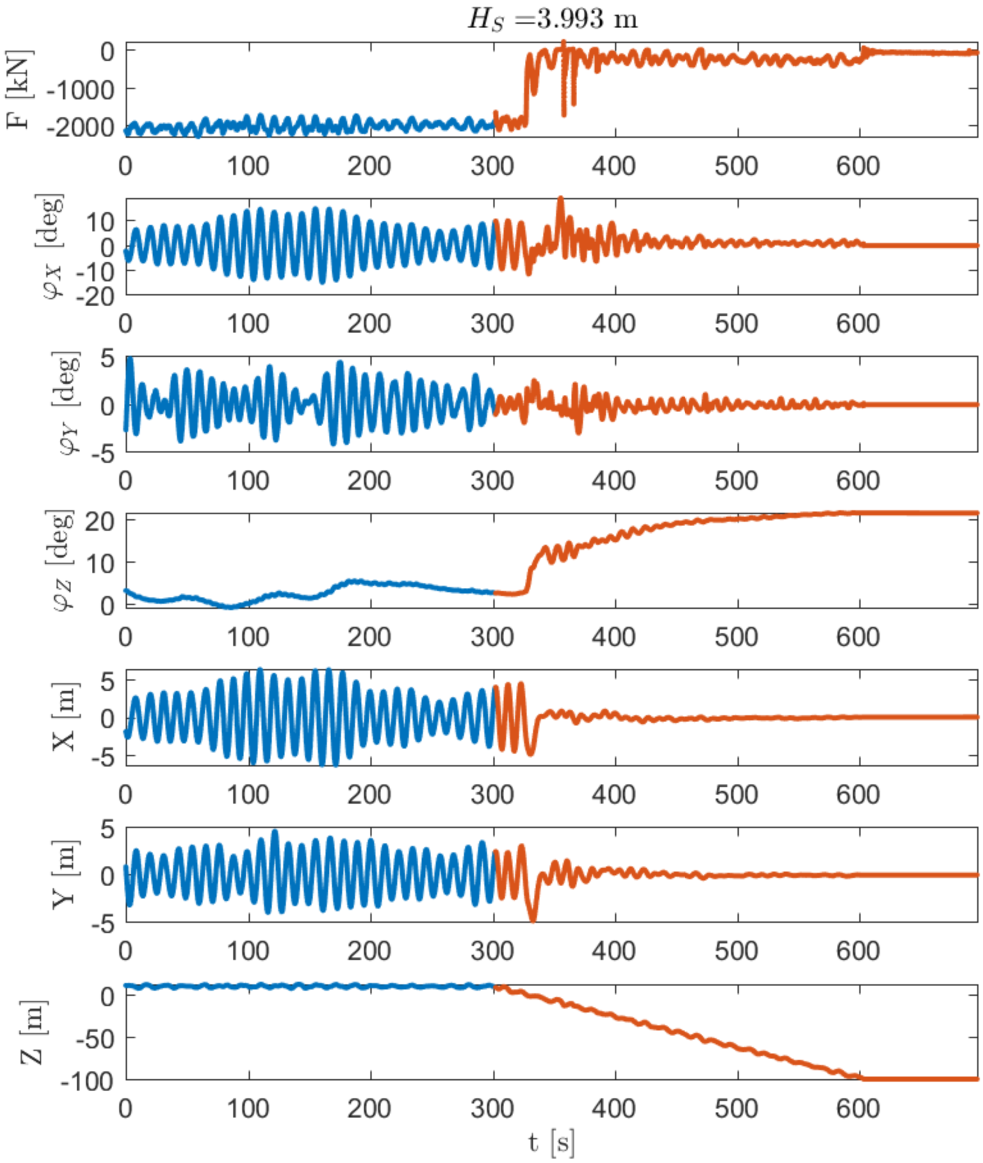

Figure 50: Example time histories for significant wave height of $H_S = 3.99\,\mathrm{m}$ for crane force F, angular displacements (pitch, roll, yaw) of the variable buoyancy anchor, φ_X, φ_Y, φ_Z and displacements of the variable buoyancy anchor along X, Y, and Z axes, respectively. Note, that time histories shown in blue correspond to anchor hanging on the crane and those shown in orange correspond to deployment stage with crane winch speed of $V_W = 0.35\,\frac{\mathrm{m}}{\mathrm{s}}$.

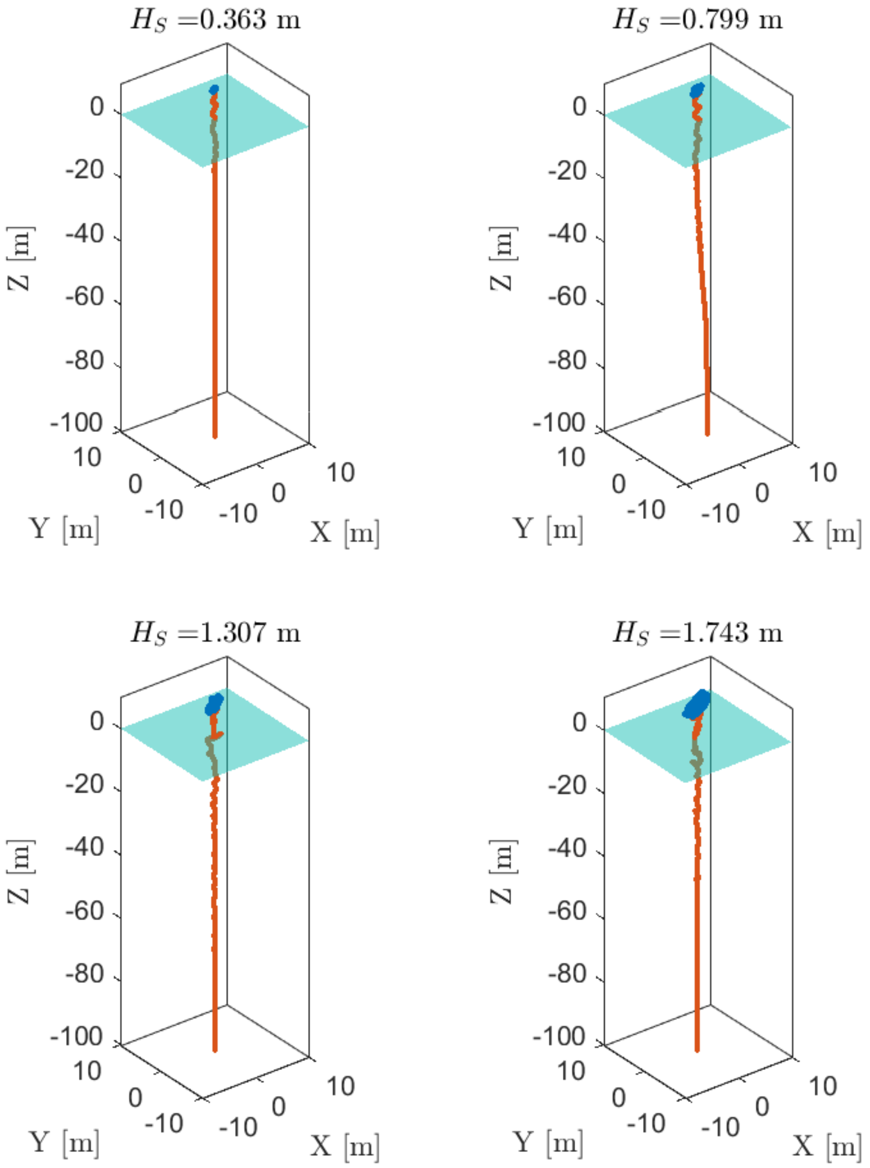

Figure 51: Example 3D trajectories of variable buoyancy anchor deployed to 100 m water depth under varying significant wave heights: $H_S = 0.36\,\mathrm{m}$, $H_S = 0.80\,\mathrm{m}$, $H_S = 1.31\,\mathrm{m}$, $H_S = 1.74\,\mathrm{m}$, respectively. Note, that trajectories shown in blue correspond to anchor hanging on the crane and those shown in orange correspond to deployment stage with crane winch speed of $V_W = 0.35\,\frac{\mathrm{m}}{\mathrm{s}}$. The plane marked in cyan colour denotes the water surface.

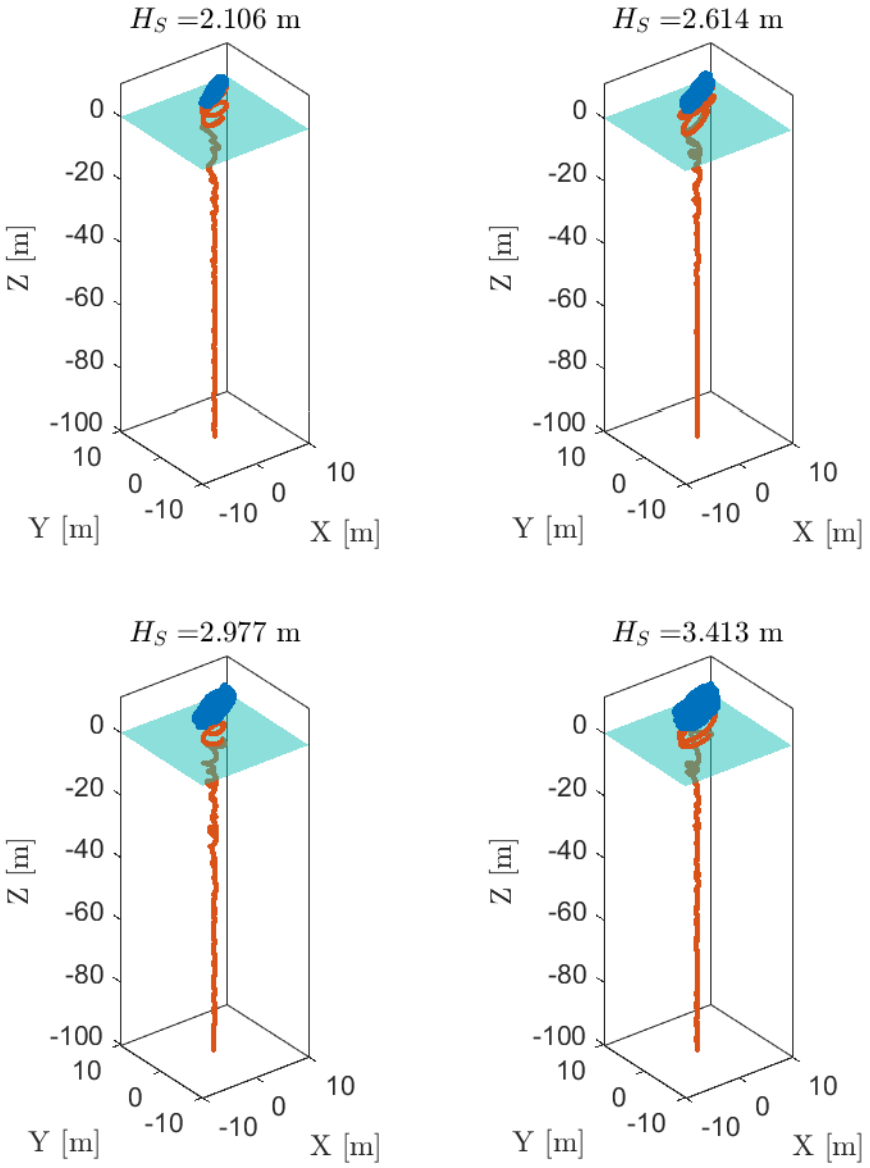

Figure 52: Example 3D trajectories of variable buoyancy anchor deployed to 100 m water depth under varying significant wave heights: $H_S = 2.11\,\mathrm{m}$, $H_S = 2.61\,\mathrm{m}$, $H_S = 2.98\,\mathrm{m}$, $H_S = 3.41\,\mathrm{m}$, respectively. Note, that trajectories shown in blue correspond to anchor hanging on the crane and those shown in orange correspond to deployment stage with crane winch speed of $V_W = 0.35\,\frac{\mathrm{m}}{\mathrm{s}}$. The plane marked in cyan colour denotes the water surface.

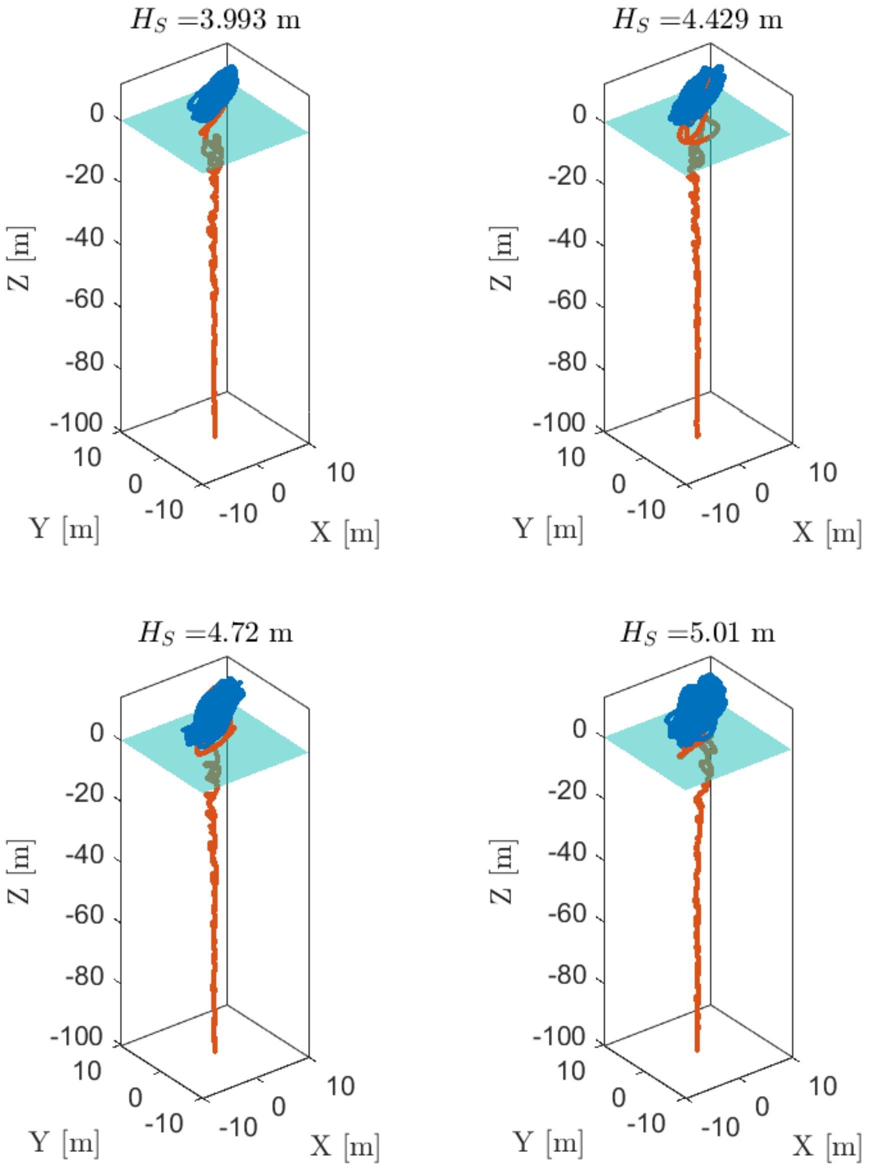

Figure 53: Example 3D trajectories of variable buoyancy anchor deployed to 100 m water depth under varying significant wave heights: $H_S = 3.99\,\mathrm{m}$, $H_S = 4.43\,\mathrm{m}$, $H_S = 4.72\,\mathrm{m}$, $H_S = 5.01\,\mathrm{m}$, respectively. Note, that trajectories shown in blue correspond to anchor hanging on the crane and those shown in orange correspond to deployment stage with crane winch speed of $V_W = 0.35\,\frac{\mathrm{m}}{\mathrm{s}}$. The plane marked in cyan colour denotes the water surface.

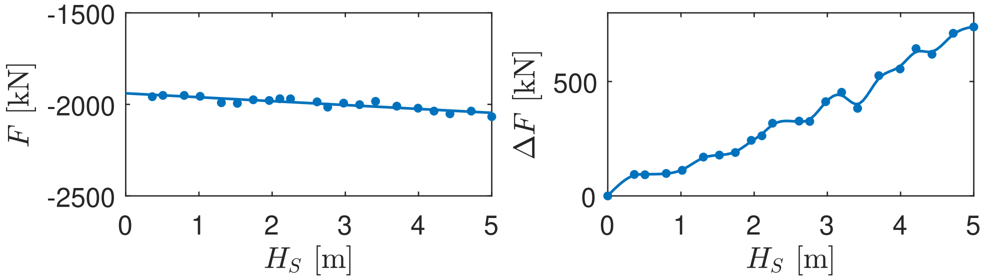

Figure 54: (Left panel) Mean force F observed by the crane winch and (Right panel) peak to peak amplitude ΔF of the winch force F as a function of significant wave height H_S (Variable bouyancy anchor suspended on the crane, pre-deployment).

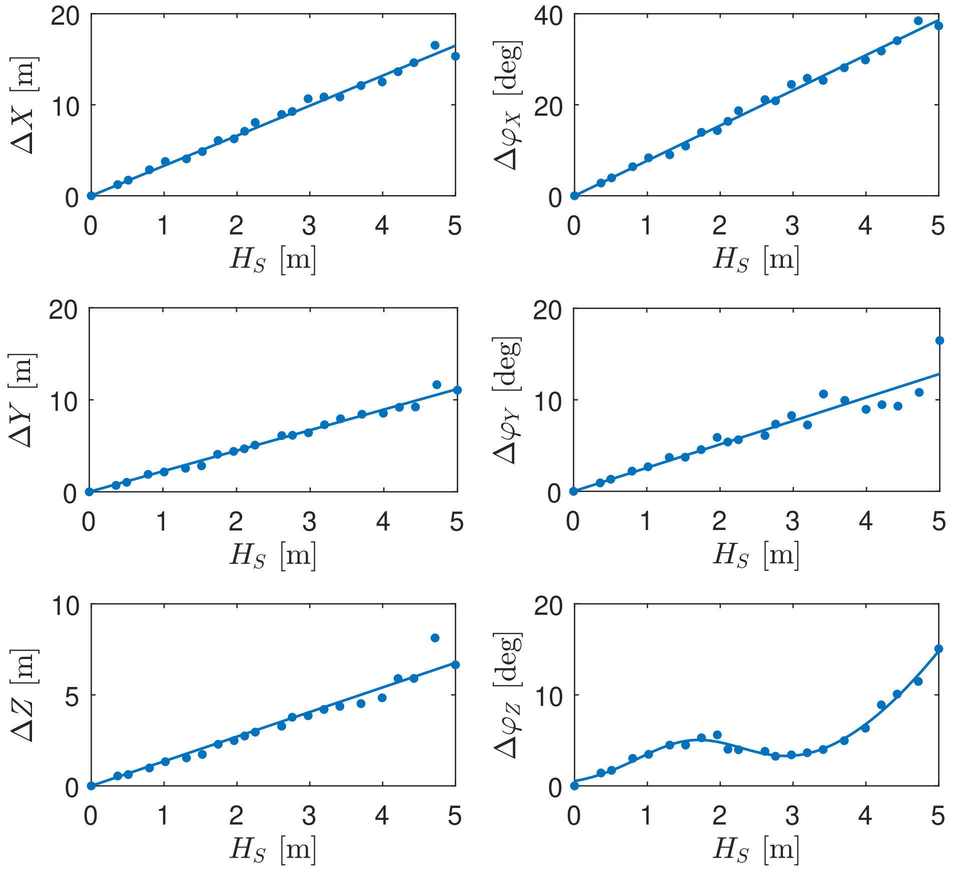

Figure 55: (Left panels) Peak to peak amplitudes of variable buoyancy anchor displacements, ΔX, ΔY, ΔZ and (Right panels) peak to peak amplitudes of angular displacements (pitch, roll, yaw) of the variable buoyancy anchor, $\Delta\varphi_X$, $\Delta\varphi_Y$, $\Delta\varphi_Z$ as a function of significant wave height H_S (Variable bouyancy anchor suspended on the crane, pre-deployment).

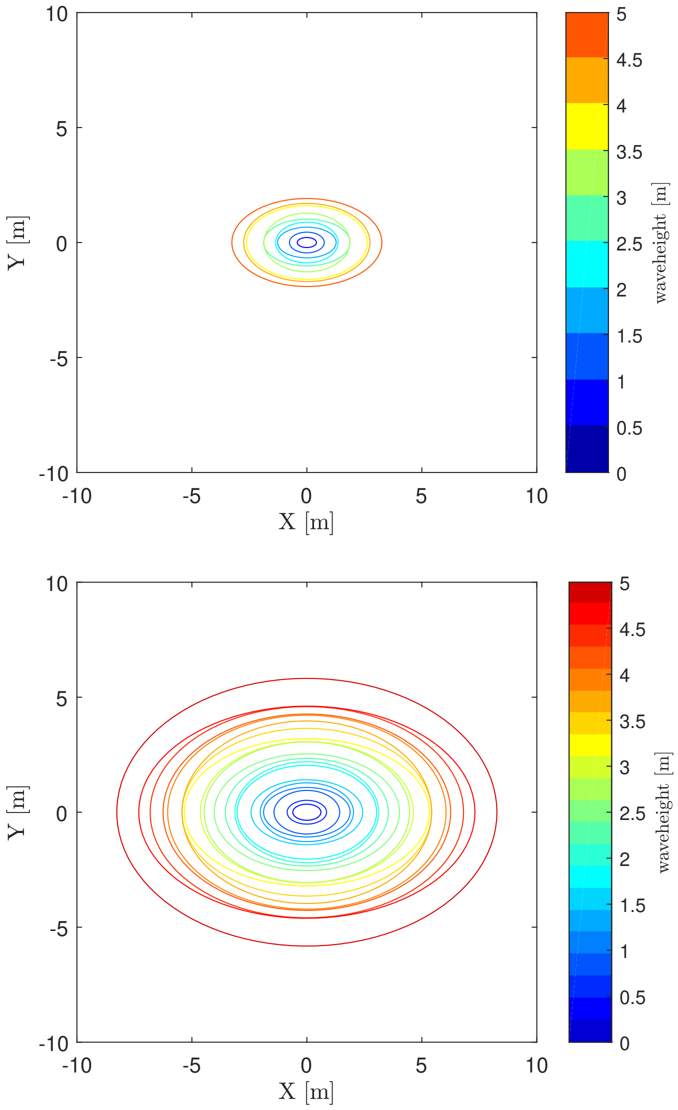

Figure 56: Maximum displacements of the suction anchor (top panel) and variable bouyancy anchor (bottom panel) suspended on the crane (pre-deployment) as a function of significant wave height H_S. Major and minor axes of the ellipses correspond to maximum displacements observed in X and Y directions.

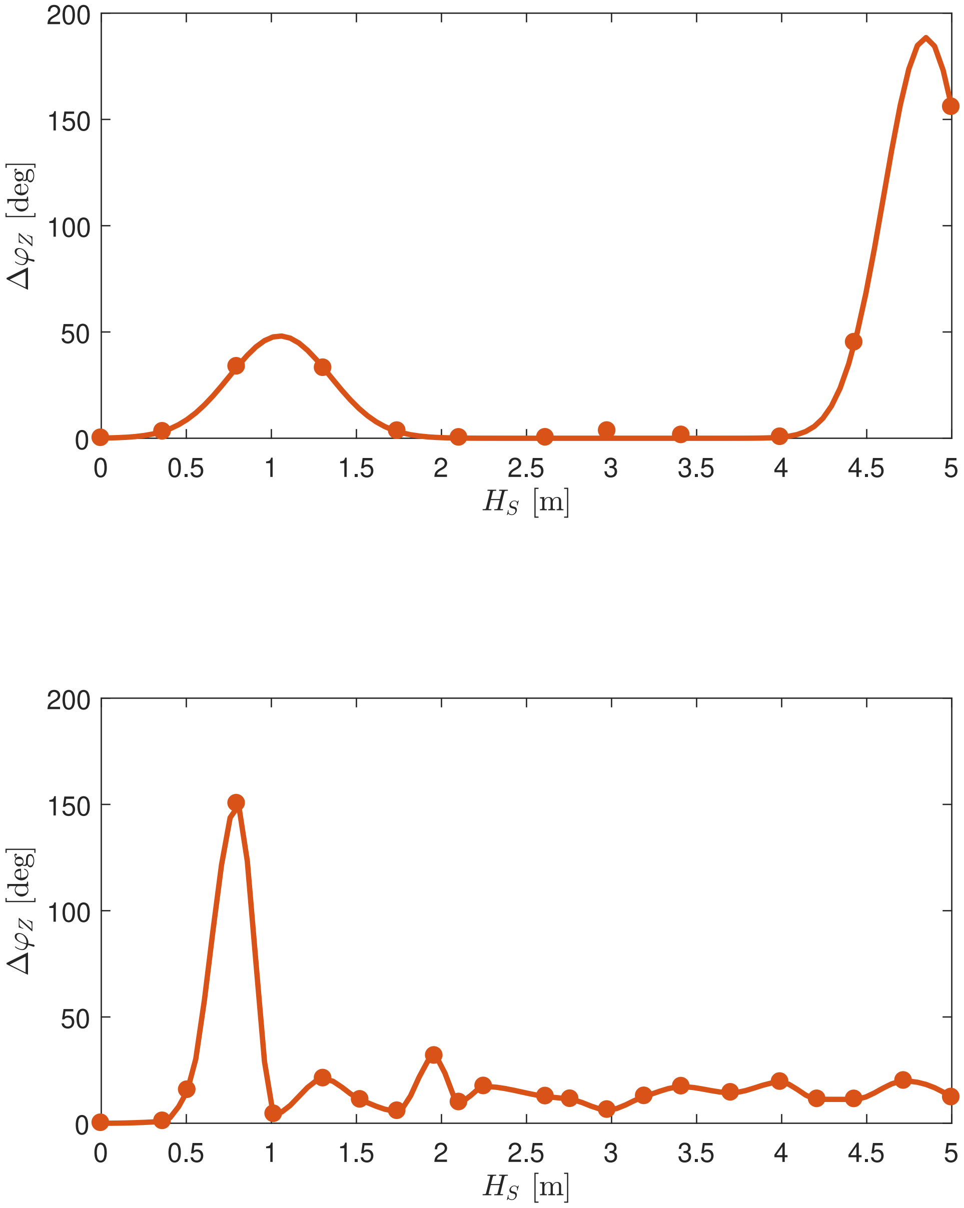

Figure 57: Comparison of yaw $\Delta\varphi_Z$ induced during deployment phase to 100m water depth (including passing through the splash zone) of suction anchor (top panel) and variable buoyancy anchor (bottom panel) as a function of significant wave height H_S.

6 Conclusions

The deployment of a novel anchor design using a real-physics simulator is described in this work. The anchor's variable buoyancy means that it can float and be towed to the deployment site. This also allows for the deployment to be done by means of a simple winch instead of a heavy-lift crane mounted on a large vessel.

The tests are divided in three main parts: buoyancy, positioning the anchor under the stern of the vessel and, descent to the seabed. The latter is subdivided in three parts: the base case with $H_S = 1$ m and $T_P = 10$ s and no ocean currents, H_S ranging from 2 to 5 m without currents and; no waves with currents ranging from 0 to 1 kn.

Buoyancy test explore the ballast pumping rate (19 different values) and its effect on the anchor's buoyancy. Data analysis found that the anchor needs approximately 4 tonnes of ballast to be fully submerged and start its descent.

Having established the anchor buoyancy limit, positioning tests are performed. In total, 2 parameters were explored, Q and H_S, amassing 174 anchor positioning simulations. The rate at which the ballast is pumped into the anchor has a direct impact on the time it takes for the anchor to position itself under the stern of the vessel, at about 20 m depth. At Q$\approx$ 1 m^3/min the anchor reaches the position in under 5 minutes, however, at the lowest Q values, it takes up to 25 minutes.

Winch force range during the positioning operations remains fairly linear at $\approx$60 kN for all pumping rates. Slow pumping rates also allow for the anchor to spend more time closer to the surface of the water, hence increasing the wave-induced anchor heave oscillations.

The base case analysis performed on the anchor dynamics during its descent consisted of 40 different tests, in which winch velocity V_W was the variable. As a first step, tests without heave compensation were performed. However, it was observed that the lack of a heave compensation system has large spikes, up to three times the values observed in the presence of heave compensation. These tests also showed that the wave-induced heave oscillations of the anchor slowed down the anchor's descent to almost 60 minutes (for slower pump rates).

In the absence of current and with just 1 m waves, the anchor drifts from its deployment location up to 10 m in the wave direction and up to 1 m in the direction normal to the waves direction at the highest winch velocities. A winch velocity of 0.35 m/s was observed to be the best in this scenario as the anchor is allowed to descend almost at free-fall whilst still being controlled by the winch. At this winch velocity, the forces acting on the winch have a working range of 30 kN.

The anchor was observed to rotate the most along its vertical axis at the slowest and fastest winch velocities. At $V_W = 0.35$ m/s however, the anchor descends almost static, with the anchor rotating almost 0°. Forces acting on the winch decrease as the winch velocity increases up to 0.35 m/s. Once this velocity is reached, the force starts to reach an equilibrium.

In comparison to the base case, the effect of waves was explored by varying V_W and H_S. A total of 66 simulations were performed for this study. In this case, the range of winch velocities tested was reduced from 0-0.58 m/s to 0.3-0.5 m/s in order to focus on the most practical range from application point of view. Compared to the base case, the increase in wave height has a marginal effect on the results. Descent takes up to 30 seconds more to reach the seabed. This due to the anchor getting "caught" in the wave orbitals that reach further down the water column. Anchor drift follows similar patterns but at the slower V_W values, the difference between the higher waves and smaller ones is up to 3 meters in the wave direction. In the direction perpendicular to the waves' propagation, the anchor drifts ±1 m from the deployment location. The anchor orientation sees little influence from the different H_S values, the most noticeable feature is the slope at which the yaw increases with V_W and H_S. As both values increase, the slope decreases. The speed at which the anchor descends levels off similarly to the base case at around 0.35 m/s. Forces acting on the winch show no relevant effect, this due to the presence of heave compensation.

On the contrary, the effect of currents on the deployment of the variable buoyancy anchor is considerably larger than that of waves. In this case, the controlled parameters were current speed and anchor weight for a total of 44 simulations. For this analysis, the drag and lift coefficients, C_D and C_L respectively, had to be calibrated. For this, the coefficients were calculated using ANSYS software and then the simulator coefficients were calibrated to match the results obtained from ANSYS.

Due to the anchor's shape and its hydrodynamics, the anchor weight increase does not have a significant effect on the descent time. However, it does have a large impact on the winch forces. A 25 t weight difference between the lightest and the heaviest anchor ballast tested gives a difference in F_W of 340 kN.

The anchor drifts from its deployment location up to 170 m in the current direction for the fastest currents and lightest ballast. On the contrary, the heaviest ballast at the fastest currents only drifts around 40 m. At the same time, currents make the anchor go up the water column, almost back to its initial position when the anchor is the lightest. For the heaviest ballast, the anchor does not move upwards. Regardless of the anchor weight, the orientation of the anchor does not change.

The comparison of crane deployment of the floating anchor and a generic suction anchor shows that the variable buoyancy anchor has significant advantages over the suction anchor. For instance, the descent to the seabed presents reduced anchor movement and reduced loads exerted on the winch. The only time the suction anchor outperforms the variable buoyancy anchor is in yaw. The floating anchor turns around its vertical axis up to double the values experienced by the suction anchor. This, however, does not have an operational issue if the angle is not large enough (e.g. 3560°) to entangle the cable and hose.

7 Project Outputs

7.1 Project presentations

- The research undertaken as part of this project has been presented to ORE Catapult and their industrial network (12th October 2021, *Project Update – Cost Effective Methods Of Installing Offshore Wind Infrastructure*). As part of follow up of meeting with ORE Catapult, we have prepared a questionnaire for the participants to comment on project progress and verify simulation assumptions (deployment depths, deployment plan, environmental parameters). This allowed us to verify model assumptions, ranges of parameters studied, in turn ensuring the modelling effort is within applicable offshore conditions and industry practice.

- Supergen Annual Assembly, 18th - 20th January 2022, University of Plymouth (Online), UK.
- Applied Dynamics and Structures & Solid Mechanics and Materials research groups seminar series, 20th April 2022, School of Engineering, University of Aberdeen, UK.
- WMVC 2022, The 10th international Conference on Wave Mechanics and Vibrations, 4 -6 July 2022, Lisbon, Portugal.
- The 9th PRIMaRE Conference, 6-7 April 2022, University of Exeter, Penryn, UK.
- PGCon: Edinburgh Postgraduate Conference, 11th July 2022, University of Edinburgh, UK.
- Royal Academy of Engineering, *Sino-British Engineering Technology Cooperation - Decarbonisation Workshop on Offshore Wind*, 14th July 2022, Online.

7.2 Publications and Abstracts

- Martinez, R., Arnau, S., Scullion, C., Neilson, R.D., Collins, P., Kapitaniak, M., *Deployment feasibility studies of variable buoyancy anchors for floating wind applications*, Mechanisms and Machine Science: Recent Trends in Wave Mechanics and Vibrations, 2022. [In press]
- Follow-up paper to present main results of this project is in preparation, plan is to submit to *Ocean Engineering* journal.
- Expanded journal paper based on WMVC 2022 conference paper is in preparation, plan is to submit to *Journal of Vibration Engineering & Technologies.*

In addition, 3 abstracts for international conferences have been submitted.

- Martinez, R., Arnau, S., Scullion, C., Neilson, R.D., Collins, P., Kapitaniak, M., *Variable buoyancy anchors for floating offshore wind turbines*, WindEurope Annual Event 2022, 5-7 April 2022, Bilbao, Spain. [Withdrawn as unable to attend]
- Martinez, R., Arnau, S., Scullion, C., Neilson, R.D., Kapitaniak, M., *Fast mooring deployment for floating offshore wind turbines*, The 10th international Conference on Wave Mechanics and Vibrations, 4 -6 July 2022, Lisbon, Portugal.

- Martinez, R., Arnau, S., Scullion, C., Neilson, R.D., Collins, P., Kapitaniak, M., *Deployment feasibility studies of variable buoyancy anchors for floating wind applications*, The 9th PRIMaRE Conference, 6-7 April 2022, Penryn, UK.

7.3 Follow-up funding enabled through this project

The project funded by EPSRC Supergen ORE Hub & ORE Catapult enabled us to apply for follow-up funding for the projects listed below. This project has been instrumental in establishing links between NDC and ORE Catapult which led to partnership (https://www.abdn.ac.uk/engineering/news/16035/) that allowed to fund 3 PhD projects focusing on floating wind. Each PhD project will be funded by ORE Catapult, NDC and the School of Engineering, University of Aberdeen.

- Kapitaniak, M. & Neilson, R., Offshore Renewable Energy Catapult, Floating Wind: Optimisation, Derisking & Development, Project value £90,000, Project duration: 1st March 2022 - 28th February 2026.
- Kapitaniak, M., Martinez, R. & Arnau, S., Energy Technology Partnership, ETP KEN: Optimization Of Towing Configuration For Floating Wind Farm Anchors, Project value £9,480, Project duration: 15th January-15th April 2022.

References

[1] Gordon Stewart and Michael Muskulus. A review and comparison of floating offshore wind turbine model experiments. *Energy Procedia*, 94:227–231, 2016. ISSN 1876-6102. 13th Deep Sea Offshore Wind R&D Conference, EERA DeepWind 2016.

[2] Catho Bjerkseter and Anders Agotnes. Levelised costs of energy for offshore floating wind turbine concepts. Master's thesis, Norwegian University of Life Sciences, Department of Mathematical Sciences and Technology, 2013.

[3] Rhodri James, Wen-Yu Weng, Chas Spradbery, Justin Jones, Denis Matha, Alexander Mitzlaff, R. V. Ahilan, Mike Frampton, and Miguel Lopes. Floating Wind Joint Industry Project - Phase I Summary Report. Technical report, The Carbon Trust, 2018.

[4] Dan Kyle Spearman, Sam Strivens, Denis Matha, Nicolai Cosack, Alan Macleay, Jeroen Regelink, Darren Patel, and Tim Walsh. Floating Wind Joint Industry Project - Phase II Summary Report. Technical report, The Carbon Trust, 2020.

[5] Sam Strivens, Emily Northridge, Hannah Evans, Mary Harvey, Tim Camp, and Nigel Terry. Floating Wind Joint Industry Project - Phase III Summary Report. Technical report, The Carbon Trust, 2021.

[6] Rhodri James and Marc Costa Ros. Floating offshore wind: Market and technology review. Technical report, The Carbon Trust, 2015.

[7] Maria Ikhennicheu, Mattias Lynch, Siobhan Doole, Friedemann Borisade, Denis Matha, Jose Luis Dominguez, Rubén Durán Vicente, Tim Habekost, Lizet Ramirez, Sabina Potestio, Climent Molins, and Pau Trubat. D2.1 - review of the state of the art of mooring and anchoring designs, technical challenges and identification of relevant dlcs. Technical report, WindEurope & IREC, 2020.

[8] Rich T. Walker, Joana Van Nieuwkoop-Mccall, Lars Johanning, and Richard J. Parkinson. Calculating weather windows: Application to transit, installation and the implications on deployment success. *Ocean Engineering*, 68:88–101, 2013. ISSN 00298018.

[9] M. O'Connor, T. Lewis, and G. Dalton. Weather window analysis of irish west coast wave data with relevance to operations & maintenance of marine renewables. *Renewable Energy*, 52:57–66, 2013. ISSN 09601481.

[10] Håvard Vindenes, Kjell Arild Orvik, Henrik Søiland, and Henning Wehde. Analysis of tidal currents in the north sea from shipboard acoustic doppler current profiler data. *Continental Shelf Research*, 162:1–12, 2018. ISSN 18736955.

[11] A. M. Davies and G. K. Furnes. Observed and computed m2 tidal currents in the north sea. *Journal of Physical Oceanography*, 10:237–257, 1980. ISSN 0022-3670.

[12] Brian Sellar and Gareth Wakelam. Characterisation of tidal flows at the European Marine Energy Centre in the absence of ocean waves. *Energies*, 11(1): 176, 2018. ISSN 1996-1073.

[13] Duncan R. J. Sutherland, Brian G. Sellar, Samuel Harding, and Ian Bryden. Initial flow characterisation utilising turbine and seabed installed acoustic sensor arrays. In *Proceedings of the 10th European Wave and Tidal Energy Conference*, pages 1–8, Aalborg, 2013.

[14] Hasselmann K., T.P. Barnett, E. Bouws, H. Carlson, D.E. Cartwright, K. Enke, J.A. Ewing, H. Gienapp, D.E. Hasselmann, P. Kruseman, A. Meerburg, P. Mller, D.J. Olbers, K.Richter, W. Sell, and H. Walden. Measurements of wind-wave growth and swell decay during the joint north sea wave project (jonswap). In *Ergnzungsheft zur Deutschen Hydrographischen Zeitschrift Reihe*, page 95, 1 1973. A(8) (Nr. 12).

[15] Willard J. Pierson Jr. and Lionel Moskowitz. A proposed spectral form for fully developed wind seas based on the similarity theory of s. a. kitaigorodskii. *Journal of Geophysical Research (1896-1977)*, 69(24):5181–5190, 1964. doi: https://doi.org/10.1029/JZ069i024p05181. URL `https://agupubs.onlinelibrary.wiley.com/doi/abs/10.1029/JZ069i024p05181`.

[16] Stephen Bull. Suction anchors for floating wind mooring cables, 5 2017. URL `https://twitter.com/newenergybull/status/859653692408160256?s=20&t=GGcHiScPpDeXVdLuWQIUQg`.

[17] Vessel Finder. Onyx - offshore support vessel, imo 9664706, 5 2022. URL `https://www.vesselfinder.com/vessels/ONYX-IMO-9664706-MMSI-538009865`.

[18] Vessel Finder. Deep explorer - offshore support vessel, imo 9729726, 5 2022. URL `https://www.vesselfinder.com/vessels/DEEP-EXPLORER-IMO-9729726-MMSI-311000411`.

[19] Adnan Memija. Dof subsea installs suction anchors on world's largest floating offshore wind farm, 5 2022. URL `https://www.offshorewind.biz/2022/05/20/dof-subsea-installs-suction-anchors-on-worlds-largest-floating-offshore-wind-farm/`.

[20] Equinor. Hywind scotland. URL `https://www.equinor.com/content/dam/statoil/documents/newsroom-additional-documents/news-attachments/brochure-hywind-a4.pdf`.